

Petrogenesis of the Early Eocene adakitic rocks in the Napuri area, southern Lhasa: Partial melting of thickened lower crust during slab break-off and implications for crustal thickening in southern Tibet



Lin Ma ^{a,b}, Bao-Di Wang ^{c,d}, Zi-Qi Jiang ^a, Qiang Wang ^{a,*}, Zheng-Xiang Li ^e, Derek A. Wyman ^f, Shou-Ren Zhao ^d, Jin-Hui Yang ^g, Guo-Ning Gou ^{a,b}, Hai-Feng Guo ^{a,b}

^a State Key Laboratory of Isotope Geochemistry, Guangzhou Institute of Geochemistry, Chinese Academy of Sciences, Guangzhou 510640, China

^b University of Chinese Academy of Sciences, Beijing 100049, China

^c Chengdu Institute of Geology and Mineral Resources, Chengdu 610081, China

^d Geological Survey Party, Institute of the Autonomous Region, Lhasa 851400, Tibet, China

^e ARC Centre of Excellence for Core to Crust Fluid Systems (CCFS) and The Institute for Geoscience Research (TIGeR), Department of Applied Geology, Curtin University, GPO Box U1987, Perth, WA 6845, Australia

^f School of Geosciences, The University of Sydney, NSW 2006, Australia

^g Institute of Geology and Geophysics, Chinese Academy of Science, Beijing 100029, China

ARTICLE INFO

Article history:

Received 5 October 2013

Accepted 16 February 2014

Available online 24 February 2014

Keywords:

Adakitic rocks

Lower crustal melting

Crustal thickening

Slab breakoff

Tibet

ABSTRACT

Cenozoic adakitic rocks in the Lhasa block (southern Tibet) have been widely used to trace the lateral extent of crustal thickening. However, their petrogenesis remains controversial. Here, we report geochronological and geochemical data for the Napuri intrusive rocks in the core area of the Quxu batholith, southern Lhasa. Zircon U–Pb dating suggests that they were generated at approximately 48 Ma. The studied samples show significant geochemical variations, manifested by the coexistence of three types of igneous rocks. Groups I and II rocks exhibit variable and high SiO₂ (66.4–73.9 wt.%), high Al₂O₃ (14.0–17.4 wt.%), K₂O (3.9–5.3 wt.%), Sr (273–718 ppm) and Sr/Y (18.3 to 81.3) values, and low Y (3.6 to 16 ppm), heavy rare earth element (REE) (e.g., Yb = 0.48 to 1.8 ppm), MgO (0.4–1.0 wt.%), Cr (2.9–7.4 ppm) and Ni (1.6–4.5 ppm) contents, which are similar to those of thickened lower crust-derived adakitic rocks. The Group I rocks show higher Sr/Y (77.5–81.3) ratios and lower total REE (55.5–63.2 ppm) contents with clearly positive Eu and Sr anomalies, whereas the Group II rocks have relatively lower Sr/Y (18.3–65.7) ratios and higher total REE (115–375 ppm) contents with negligible or slightly negative Eu and Sr anomalies. Group III rocks have the highest SiO₂ (74.5–76.0 wt.%), Y (17.0–23.7 ppm) and Yb (2.91–3.30 ppm) contents, and the lowest Al₂O₃ (12.5–13.2 wt.%), Sr (81.3–141 ppm) and Sr/Y (4.8–5.9) values with distinctly negative Eu and Sr anomalies. Compared with the Jurassic–Cretaceous granitoids in southern Lhasa, the relative enrichment in Sr–Nd–Hf isotopic compositions (⁸⁷Sr/⁸⁶Sr)_i = 0.7049–0.7055, ε_{Nd(t)} = −0.3 ± 0.7 and ε_{Hf(t)}_{zircon} = +3.6 ± 11.4) for the Napuri intrusive rocks indicates that they likely contained Indian continental components. The Group I and Group II rocks most probably originated from thickened mafic lower crust (amphibolite eclogites or garnet amphibolites) with garnet + rutile ± plagioclase as residual minerals in the source at >1.5 GPa, corresponding to depths of >50 km, and Group III rocks were probably generated by fractional crystallization of plagioclase from the adakitic magmas. Taking into account the narrow linear nature of the Eocene magmatic belt and reported synchronous asthenosphere-derived basaltic rocks in southern Lhasa, we suggest that upwelling asthenosphere triggered by the break-off of subducted Neo-Tethyan slab probably provided the required thermal conditions for lower crustal melting. The identification of Indian continental components in the Napuri intrusive rocks probably indicates that the Asia–India collision had taken place prior to their emplacement. The dramatic changes in the (La/Yb)_N ratios and ε_{Nd(t)} and ε_{Hf(t)} values of magmatic rocks in the Gangdese area at ca. 51–46 Ma indicate that the Cenozoic crustal thickening associated with the indentation of the Indian continent began in the Early Eocene (ca. 51–46 Ma) at the latest.

© 2014 Elsevier B.V. All rights reserved.

1. Introduction

The Tibetan Plateau has the thickest continental crust on Earth. Various models have been proposed in the past decades to account for the formation of the plateau, which can be roughly summarized as

* Corresponding author.

E-mail address: wqiang@gig.ac.cn (Q. Wang).

crustal/lithospheric thickening models (e.g., Tapponnier et al., 2001; Wang et al., 2008; Yin and Harrison, 2000), convective removal or delamination of the lower lithosphere models (e.g., Chung et al., 1998, 2009; Turner et al., 1996) and crustal flow models (e.g., Royden et al., 1997; Wang et al., 2012). The timing and mechanism of the continental crustal thickening are pivotal factors that all such models need to reconcile.

Cenozoic adakitic rocks are widely distributed in a 1500 km-long E–W trending magmatic belt in southern Lhasa, the southern Tibetan Plateau (e.g., Chung et al., 2003, 2005, 2009; Gao et al., 2010; Guo et al., 2007; Hou et al., 2004, 2012 and references therein) and have been widely used for tracing crustal thickening processes in the region (e.g., Chung et al., 2003, 2009; Guan et al., 2012; Hou et al., 2012; Ji et al., 2012; Zeng et al., 2011). Nonetheless, their petrogenesis remains a highly controversial issue. Various magmatic sources have been proposed to account for the generation of these adakitic rocks, including a thickened mafic lower continental crust (e.g., Chung et al., 2003; Guan et al., 2012; Guo et al., 2007; Hou et al., 2004; Ji et al., 2012), subducted Indian continental crust (e.g., Xu et al., 2010), upper mantle metasomatized by slab-derived melts (e.g., Gao et al., 2007, 2010), and Jurassic–Eocene Gangdese intermediate intrusive rocks and basement metasedimentary rocks (e.g., King et al., 2007; Pan et al., 2012; Zhang et al., 2010a).

The Cenozoic adakitic rocks in southern Lhasa were mainly emplaced between the Late Oligocene and the Late Miocene (ca. 26–9 Ma; Chung et al., 2003; Guo et al., 2007; Hou et al., 2004). More recently, Eocene–Oligocene (ca. 51–30 Ma) adakitic rocks have also been reported (e.g., Chung et al., 2009; Guan et al., 2012; Hou et al., 2012; Ji et al., 2012; Jiang et al., 2011; Zeng et al., 2011). In this study, we present detailed petrology, geochronology, mineral composition, and major and trace element and Sr–Nd–Hf isotopic data for the Napuri adakitic intrusive rocks at the hinterland of the Quxu batholith in southern Lhasa (Fig. 1). New SHRIMP (Sensitive High Resolution Ion Microprobe) and LA-ICPMS (Laser Ablation Inductively Coupled Plasma Mass Spectrometry) zircon U–Pb dating results indicate that they were generated in the early Eocene (49–46 Ma). Owing to the wide occurrence of Early Cenozoic adakitic rocks in southern Tibet, a better understanding of their petrogenesis has importance for delineating the processes of Cenozoic crustal thickening and plateau uplift in southern Tibetan.

2. Geological background and rock characteristics

From south to north, Tibet consists of the Himalaya, Lhasa, Qiangtang, Songpan-Ganze, and Kunlun-Qaidam blocks (Yin and Harrison, 2000). The Lhasa block is bounded by the Indus–Yarlung Tsangpo suture (IYTS) to the south and the Bangong–Nujiang suture (BNS) to the north (Fig. 1a) (Yin and Harrison, 2000). It is generally accepted that the BNS developed during the Late Jurassic–Middle Cretaceous (Yin and Harrison, 2000). The IYTS marks the closure of the Tethys, and lies on the southern boundary of an east–west-trending Andean arc-type calc-alkaline magmatic zone (including the Yeba, Sangri, Linzizong volcanic successions and the Gangdese batholith) in the Lhasa block (Fig. 1a) (e.g., Coulon et al., 1986; Mo et al., 2007; Zhu et al., 2008).

The Gangdese batholith, consisting of the Latest Triassic–Late Miocene intermediate–felsic intrusive rocks, is one of the most important geologic units of southern Lhasa (e.g., Chu et al., 2006; Chung et al., 2003, 2009; Ji et al., 2009, 2012; Wen et al., 2008a,b). The adakitic intrusive rocks within the Gangdese batholith are considered to have been generated in two main stages, the Jurassic–Cretaceous (160–77 Ma) and Paleocene–Miocene (62–10 Ma): (1) Jurassic–Cretaceous adakitic rocks generated in an arc setting were related to Neo-Tethyan subduction processes, by melting of either subducted oceanic slabs (e.g., Jiang et al., 2012; Ma et al., 2013a; Wei et al., 2007; Zhang et al., 2010b; Zhu et al., 2009) or thickened mafic continental lower crust (e.g., Guan et al., 2010; Wen et al., 2008b); (2) Cenozoic adakitic rocks occurring as small-volume plugs or dikes/sills, which intrude or crosscut the Gangdese batholith, the Linzizong volcanic successions and associated sedimentary formations, and extend ~1300 km across nearly the entire

southern Lhasa (Fig. 1b) (e.g., Chung et al., 2003, 2005, 2009; Gao et al., 2007, 2010; Guan et al., 2012; Guo et al., 2007; Hou et al., 2004, 2012; Ji et al., 2012; Jiang et al., 2011, 2014; Pan et al., 2012; Xu et al., 2010; Zhang et al., 2010a).

The Napuri area of Doilungdeqen County (Fig. 1c) is difficult to access due to the high altitudes (4800–5700 m). Large-scale granitic intrusive bodies, being parts of the Quxu batholith, are found in the area (Fig. 1b, c). These intrusive rocks are composed mainly of porphyritic granites, and minor quartz monzonites with a heterogeneous granular texture. A total of 12 samples were collected for this study, including 10 granites and 2 quartz monzonites. The granite is composed of plagioclase (15–25 vol.%), alkali feldspar (25–35 vol.%), quartz (30–40 vol.%), biotite (5–10 vol.%), and titanite (1–2 vol.%) with minor epidote, magnetite and titaniferous magnetite (Fig. 2a, b, e and f). The quartz monzonite consists of plagioclase (35–45 vol.%), alkali feldspar (30–40 vol.%), quartz (10–15 vol.%), biotite (5–10 vol.%), and titanite (1–2 vol.%) with minor epidote, magnetite and titaniferous magnetite (Fig. 2c and d).

3. Analytical methods

All silicate mineral analyses were carried out at the State Key Laboratory of Isotope Geochemistry, Guangzhou Institute of Geochemistry, Chinese Academy of Sciences (SKLaBIG GIG CAS) using a JXA-8100 electron microprobe. An accelerating voltage of 15 kV, a specimen current of 2.0×10^{-8} A, and a beam size of 1–2 μm were employed. The analytical errors are generally less than 2%. The analytical procedures were described in detail in Huang et al. (2007).

Zircons were separated using standard density and magnetic separation techniques. Zircon grains were handpicked and mounted in an epoxy resin disc, and then polished and coated with gold. Cathodoluminescence (CL) images were taken at SKLaBIG GIG CAS with a JEOL JXA-8100 Superprobe for inspecting the internal morphology of individual zircons and for selecting positions for U–Pb and Lu–Hf isotope analyses. U–Pb isotope compositions of zircon grains from two samples (D175 and D182) were analyzed using the SHRIMP at the John de Laeter Centre of Mass Spectrometry of Curtin University of Technology in Perth, Western Australia. Both unknown zircon grains and zircon standards, TEMORA (for calibrating the U–Th–Pb ratios; $^{206}\text{Pb}/^{238}\text{U} = 0.0668$, corresponding to 417 Ma; Black et al., 2003) and CZ3 (for calibrating absolute U abundances; U = 551 ppm; Pidgeon et al., 1994) were analyzed under the following conditions: cycles of 7 scans, primary O_2^- beam of ~2 nA, spot size of ~25 μm with a mass resolution of about 5000. The data have been reduced following the procedure described by Williams (1998) using the software SQUID (Ludwig, 2001). U/Pb ratios and U concentrations of the samples have been normalized to the TEMORA and CZ3 standards, respectively. Common Pb was determined using measured ^{204}Pb and by applying a composition after Stacey and Kramers (1975) appropriate to the age of the zircon. LA-ICPMS zircon U–Pb dating for sample PIII-02 were conducted at the MC-ICPMS laboratory of the Institute of Geology and Geophysics, Chinese Academy of Sciences (IGG CAS) in Peking, China. Detailed operating conditions for the laser ablation system and the ICP-MS instrument and data reduction were the same as described by Xie et al. (2008). An Agilent 7500a quadrupole (Q)-ICPMS and a Neptune multi-collector (MC)-ICPMS with a 193 nm excimer ArF laser-ablation system (GeoLas Plus) attached were used for simultaneous determination of zircon U–Pb ages. In situ Hf isotope measurements were subsequently done using LA-ICPMS with a beam size of 60 μm and laser pulse frequency of 8 Hz with age determinations at the MC-ICPMS laboratory of IGG CAS. Details of instrumental conditions and data acquisition were given in Wu et al. (2006). The isobaric interference of ^{176}Lu on ^{176}Hf is negligible due to the extremely low $^{176}\text{Lu}/^{177}\text{Hf}$ in zircon (normally <0.002).

Rock samples were examined by optical microscopy and selected whole-rock samples were sawed into small chips and ultrasonically cleaned in distilled water with <3% HNO_3 and then in distilled water alone and subsequently dried and handpicked to remove visible alteration. The rocks were powdered in a chrome ring mill, and the resulting

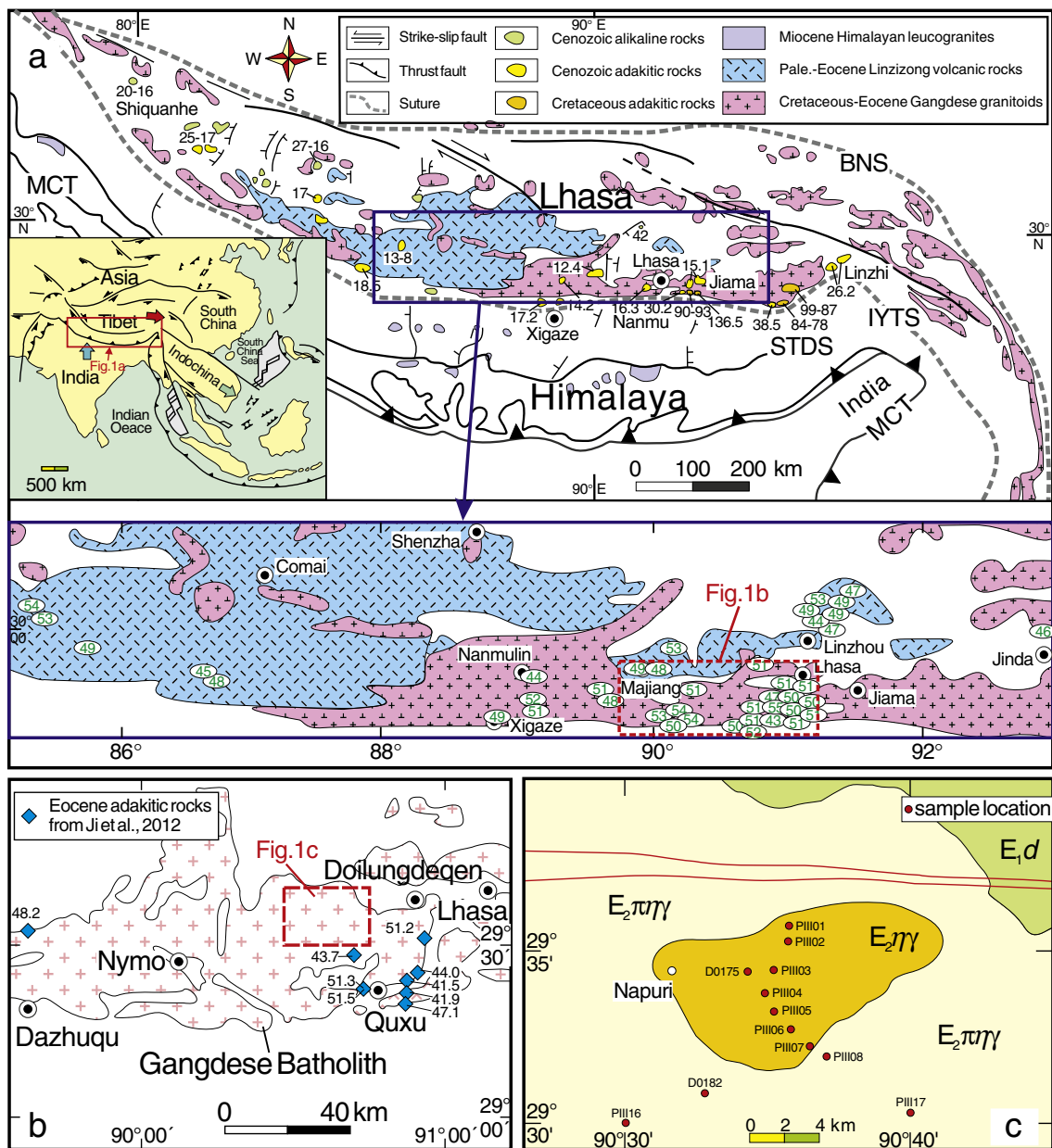


Fig. 1. (a) Geological map of the Lhasa block (modified from Chung et al. (2009)), with numbers showing ages (Ma) of Cretaceous and Cenozoic adakitic and potassic magmatism (Chung et al., 2003; Gao et al., 2007, 2010; Guan et al., 2010, 2012; Guo et al., 2006, 2007; Hou et al., 2004; Ji et al., 2012; Jiang et al., 2012; Ma et al., 2013a; Wen et al., 2008b; Xu et al., 2010; Zhang et al., 2010a,b; Zhu et al., 2009). The age data of early Eocene igneous rocks in southern Lhasa are from Ji et al. (2009), Lee et al. (2009) and Wen et al. (2008b). BNSZ = the Bangong-Nujiang suture; IYTS = the Indus-Yarlung Tsangpo Suture; MCT = the Main Central Thrust; STDS = the South Tibet Detachment System. (b) Map of the Quxu batholith showing locations of previously reported Cenozoic adakitic rocks in the literature (modified from Ji et al. (2012)), and the study region. (c) Geological map of the Napuri area, southern Tibet, showing the sampling locations. The rock type in Fig. 1c: E₁d = the Paleocene Dianzhong Group; E₂πγ = Eocene porphyritic quartz monzonite; E₂πγγ = Eocene porphyritic granite.

powders were used for analyses of major and trace elements, and Sr-Nd isotopes, at SKLaBIG GIG CAS. Major-element oxides were analyzed using a Rigaku RIX 2000 X-ray fluorescence spectrometer at SKLaBIG GIG-CAS on fused glass beads. Calibration lines used in quantification were produced by bivariate regression of data from 36 reference materials encompassing a wide range of silica compositions (Li et al., 2005), and analytical uncertainties are between 1% and 5%. Trace elements were analyzed by inductively coupled plasma mass spectrometry (ICP-MS), using a Perkin-Elmer Scielex ELAN 6000 instrument at SKLaBIG GIG CAS. Analytical procedures are the same as those described by Li et al. (2002). Repeated runs give <3% RSD (relative standard deviation) for most elements of reference materials analyzed by ICP-MS.

Sr and Nd isotopic ratios of selected samples were determined using a Micromass Isoprobe multi-collector mass spectrometer (MC-ICP-MS)

at SKLaBIG GIG-CAS. Analytical procedures are similar to those described in Wei et al. (2002) and Li et al. (2004). The $^{87}\text{Sr}/^{86}\text{Sr}$ ratio of the NBS987 standard and $^{143}\text{Nd}/^{144}\text{Nd}$ ratio of the Shin Etsu JNd-1 standard measured were 0.710285 ± 15 (2σ m) and 0.512085 ± 10 (2σ m), respectively. All measured $^{143}\text{Nd}/^{144}\text{Nd}$ and $^{86}\text{Sr}/^{88}\text{Sr}$ ratios are fractionation corrected for mass fractionation using $^{146}\text{Nd}/^{144}\text{Nd} = 0.7219$ and $^{86}\text{Sr}/^{88}\text{Sr} = 0.1194$, respectively.

4. Results

4.1. Zircon U-Pb geochronology

The zircon U-Pb isotopic data are given in Table 1. The zircons from three Napuri intrusive rock samples have crystal lengths of

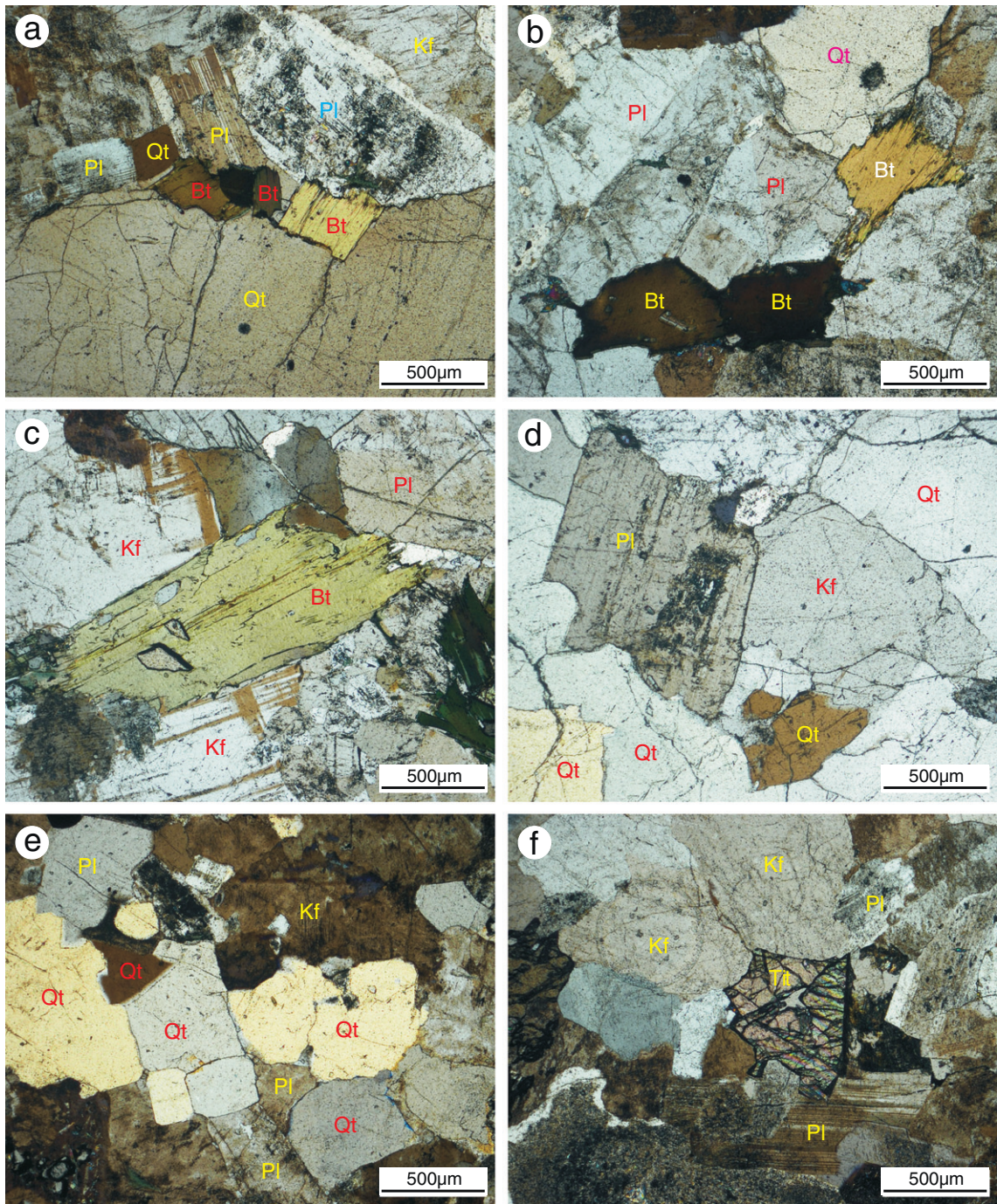


Fig. 2. Petrography (plane-polarized light) of the Napuri intrusive rocks: (a–b) sample D0175; (c–d) sample PIII-8; (e–f) sample PIII-1. Abbreviations: Pl, plagioclase; Kf, potassium feldspar; Bt, biotite; Tit, titanite; Qt, quartz.

~100–150 μm with length-to-width ratios of 2:1 to 3:1 (Fig. 3). The analyzed zircon grains from three samples have variable U (129–5039 ppm) and Th (86–1686 ppm) contents, with Th/U ratios ranging from 0.41 to 2.00, indicating a magmatic origin (Hoskin and Black, 2000).

Except for one analyzed spot with an old inheritance age (83.0 Ma), SHRIMP zircon U-Pb analyses of eighteen other spots of sample D0175 gave $^{206}\text{Pb}/^{238}\text{U}$ ages of 43 to 48 Ma, with a weighted mean age of 46.1 ± 0.6 Ma (2σ error, and the same for all other age data; Fig. 3a). Sixteen zircon SHRIMP U-Pb analyses (one for each zircon) of sample D0182 yielded $^{206}\text{Pb}/^{238}\text{U}$ ages of 47 to 51 Ma, with a weighted mean age of 48.2 ± 0.6 Ma (Fig. 3b). Ten LA-ICP-MS zircon U-Pb analyses of zircons from sample PIII-2 gave $^{206}\text{Pb}/^{238}\text{U}$ ages of 45 to 49 Ma with a weighted mean age of 47.4 ± 0.9 Ma (Fig. 3c). Thus, in-situ zircon

U-Pb dating of three samples suggests that these rocks were generated in the Early Eocene (48–46 Ma) (Fig. 3, Table 1), broadly contemporaneous with the Early Eocene (52–49 Ma) adakitic rocks from other areas in southern Lhasa (Ji et al., 2012; Zhang et al., 2010a).

4.2. Mineral geochemistry

Major oxide data for plagioclase, potassium feldspar, titanite, biotite and magnetite are listed in Table 2. Plagioclase in the Napuri intrusive rocks mainly consists of oligoclase ($\text{An}_{28-16}\text{Ab}_{70-81}\text{Or}_{3-1}$) and minor albite ($\text{An}_{6-1}\text{Ab}_{92-98}\text{Or}_{2-0}$) and andesine ($\text{An}_{35}\text{Ab}_{63}\text{Or}_2$) (Table 2). Potassium feldspar has composition of $\text{Ab}_{3-8}\text{Or}_{92-97}$. Biotite has moderate TiO_2 contents (2.2–2.3 wt.%, Table 2).

Table 1

SHRIMP II and LA-ICP-MS zircon U–Pb isotopic analyses for the Napuri granitoids.

Analysis	Content (ppm)		Isotopic ratios						Isotopic ages (Ma)						
	Th	U	Th/U	$^{207}\text{Pb}/^{206}\text{Pb}$	$\pm 1\sigma$	$^{207}\text{Pb}/^{235}\text{U}$	$\pm 1\sigma$	$^{206}\text{Pb}/^{238}\text{U}$	$\pm 1\sigma$	$^{207}\text{Pb}/^{206}\text{Pb}$	$\pm 1\sigma$	$^{207}\text{Pb}/^{235}\text{U}$	$\pm 1\sigma$	$^{206}\text{Pb}/^{238}\text{U}$	$\pm 1\sigma$
<i>D0182 (SHRIMP II)</i>															
1	86	160	0.54	0.0342	0.0040	0.0344	0.0044	0.0073	0.0004	-107	154	34.0	4.0	47.0	2.0
2	255	270	0.94	0.0332	0.0076	0.0335	0.0077	0.0073	0.0001	-150	267	33.0	8.0	47.1	0.7
3	360	877	0.41	0.0460	0.0019	0.0469	0.0022	0.0074	0.0002	-3	60	47.0	2.0	48.0	1.0
4	311	353	0.88	0.0465	0.0039	0.0505	0.0058	0.0079	0.0006	26	121	50.0	6.0	51.0	4.0
5	405	451	0.90	0.0459	0.0027	0.0495	0.0029	0.0078	0.0001	-7	107	49.0	3.0	50.2	0.5
6	1559	1042	1.50	0.0471	0.0024	0.0470	0.0027	0.0072	0.0002	52	77	47.0	3.0	47.0	1.0
7	167	265	0.63	0.0151	0.0089	0.0151	0.0090	0.0073	0.0003	-1029	493	15.0	9.0	47.0	2.0
8	506	634	0.80	0.0438	0.0110	0.0453	0.0114	0.0075	0.0002	-83	356	45.0	11.0	48.0	1.0
9	422	393	1.07	0.0340	0.0106	0.0348	0.0109	0.0074	0.0001	-115	388	35.0	11.0	47.7	0.6
10	239	279	0.86	0.0361	0.0044	0.0371	0.0049	0.0074	0.0004	-29	242	37.0	5.0	48.0	2.0
11	293	429	0.68	0.0450	0.0029	0.0466	0.0035	0.0075	0.0003	-22	91	46.0	3.0	48.0	2.0
12	405	464	0.87	0.0524	0.0031	0.0545	0.0033	0.0075	0.0001	305	120	54.0	3.0	48.4	0.5
13	200	207	0.97	0.0385	0.0125	0.0403	0.0132	0.0076	0.0003	-377	433	40.0	13.0	49.0	2.0
14	370	437	0.85	0.0452	0.0036	0.0460	0.0037	0.0074	0.0001	-12	154	46.0	4.0	47.5	0.5
15	319	357	0.90	0.0402	0.0053	0.0421	0.0055	0.0076	0.0001	-279	206	42.0	5.0	48.8	0.6
16	293	264	1.11	0.0404	0.0039	0.0411	0.0042	0.0074	0.0003	-265	148	41.0	4.0	47.0	2.0
<i>D0175 (SHRIMP II)</i>															
1	1210	1673	0.72	0.0450	0.0034	0.0457	0.0035	0.0074	0.0001	-21	147	45.0	3.0	47.3	0.5
2	304	223	1.36	0.0308	0.0121	0.0304	0.0120	0.0072	0.0001	-251	469	30.0	12.0	46.0	0.8
3	724	822	0.88	0.0473	0.0073	0.0481	0.0075	0.0074	0.0001	65	269	48.0	7.0	47.3	0.7
4	186	189	0.98	0.0119	0.0111	0.0115	0.0108	0.0070	0.0001	-1216	663	12.0	11.0	45.2	0.8
5	398	244	1.63	0.0452	0.0118	0.0452	0.0118	0.0073	0.0001	-11	390	45.0	11.0	46.7	0.8
6	196	129	1.51	0.0355	0.0074	0.0332	0.0071	0.0068	0.0002	-55	265	33.0	7.0	44.0	1.0
7	434	528	0.82	0.0387	0.0045	0.0338	0.0040	0.0063	0.0001	-365	221	34.0	4.0	40.7	0.6
8	134	140	0.96	0.0120	0.0117	0.0215	0.0210	0.0130	0.0002	-1209	671	22.0	21.0	83.0	1.0
9	190	231	0.82	0.0235	0.0067	0.0224	0.0065	0.0069	0.0001	-587	311	23.0	6.0	44.6	0.7
10	440	221	2.00	0.0476	0.0091	0.0466	0.0089	0.0071	0.0001	80	320	46.0	9.0	45.6	0.6
11	192	164	1.17	0.0442	0.0346	0.0444	0.0347	0.0073	0.0003	-60	1072	44.0	34.0	47.0	2.0
12	154	186	0.83	0.0392	0.0069	0.0377	0.0066	0.0070	0.0001	-336	263	38.0	6.0	44.8	0.5
13	149	207	0.72	0.0319	0.0126	0.0321	0.0126	0.0073	0.0001	-201	482	32.0	12.0	46.8	0.8
14	106	130	0.82	0.0187	0.0123	0.0171	0.0113	0.0066	0.0002	-829	630	17.0	11.0	43.0	1.0
15	276	424	0.65	0.0336	0.0050	0.0332	0.0049	0.0072	0.0001	-130	187	33.0	5.0	46.0	0.5
16	406	312	1.30	0.0070	0.0124	0.0068	0.0121	0.0071	0.0001	-1523	762	7.0	12.0	45.4	0.8
19	373	282	1.32	0.0121	0.0131	0.0119	0.0128	0.0071	0.0001	-1200	718	12.0	13.0	45.7	0.8
20	234	164	1.43	0.0563	0.0059	0.0578	0.0061	0.0074	0.0001	463	219	57.0	6.0	47.8	0.5
21	377	452	0.83	0.0391	0.0244	0.0378	0.0236	0.0070	0.0002	-342	921	38.0	23.0	45.0	1.0
22	106	145	0.73	0.0218	0.0133	0.0216	0.0132	0.0072	0.0002	-668	644	22.0	13.0	46.1	1.0
<i>PIII-02 (LA-ICPMS)</i>															
1	847	1600	0.53	0.0563	0.0062	0.0574	0.0061	0.0074	0.0002	465	251	57.0	6.0	47.0	1.0
2	847	761	1.11	0.1315	0.0134	0.1608	0.0156	0.0089	0.0003	2119	185	151.0	14.0	57.0	1.0
3	1454	5036	0.29	0.1132	0.0640	0.1847	0.1032	0.0118	0.0010	1851	1271	172.0	88.0	76.0	3.0
4	445	757	0.59	0.0612	0.0096	0.0635	0.0097	0.0075	0.0003	645	353	62.0	9.0	48.0	2.0
5	1167	1096	1.06	0.1675	0.0695	0.2286	0.0927	0.0099	0.0009	2533	1018	209.0	77.0	63.0	2.0
6	1194	1460	0.82	0.0740	0.0116	0.0767	0.0115	0.0075	0.0003	1041	338	75.0	11.0	48.0	2.0
7	754	784	0.96	0.0855	0.0057	0.1021	0.0066	0.0088	0.0002	1327	84	99.0	6.0	56.0	2.0
8	782	1117	0.70	0.0579	0.0100	0.0567	0.0096	0.0071	0.0003	525	372	56.0	9.0	46.0	2.0
9	799	750	1.06	0.1399	0.0259	0.1543	0.0277	0.0080	0.0004	2227	347	146.0	24.0	51.0	1.0
10	315	595	0.53	0.0461	0.0082	0.0448	0.0078	0.0071	0.0003	308	45.0	8.0	45.0	1.0	
11	493	1272	0.39	0.0490	0.0053	0.0493	0.0052	0.0073	0.0002	146	242	49.0	5.0	47.0	1.0
12	588	788	0.75	0.0828	0.0091	0.0843	0.0089	0.0074	0.0003	1265	139	82.0	8.0	48.0	2.0
13	1686	1559	1.08	0.1013	0.0228	0.1148	0.0256	0.0082	0.0003	1648	473	110.0	23.0	53.0	0.7
14	828	849	0.97	0.0624	0.0080	0.0625	0.0083	0.0073	0.0003	689	222	62.0	8.0	47.0	2.0
15	1299	1169	1.11	0.0682	0.0225	0.0656	0.0213	0.0070	0.0004	875	676	64.0	20.0	45.0	2.0
16	1572	1767	0.89	0.0915	0.0117	0.0965	0.0120	0.0077	0.0002	1458	256	94.0	11.0	49.0	1.0

4.3. Major and trace element geochemistry

Chemical composition data of eleven Napuri samples are listed in Table 3. The samples mainly plot in the granite field, except for two in the quartz monzonite field (Fig. 4a). They have variable SiO_2 (66.4–76.0 wt.%) and Al_2O_3 (12.5–17.4 wt.%) and high K_2O (3.6–5.3 wt.%) and Na_2O (3.5–4.8 wt.%) contents with $\text{K}_2\text{O}/\text{Na}_2\text{O} = 0.80$ –1.56 (Table 3), and are high-K calc-alkaline and low-Fe (Fig. 4b–c). Apart from sample PIII-4 with peraluminous characteristics ($[\text{A}/\text{CNK} = \text{Al}^{3+}/\text{Ca}^{2+} + \text{Na}^{+} + \text{K}^{+}] = 1.12$), the samples are metaluminous to slightly peraluminous ($\text{A}/\text{CNK} = 0.97$ –1.03) (Fig. 4d).

All of the samples are characterized by low MgO (0.3–1.0 wt.%), Cr (1.1–7.4 ppm) and Ni (0.9–4.5 ppm) contents (Table 3; Fig. 3e–f).

On chondrite-normalized REE diagrams, the Napuri rocks show variable patterns with slightly enriched light REEs (LREEs) ($[\text{La/Yb}]_{\text{N}} = 5$ –100) and slightly depleted heavy REEs (HREEs) ($[\text{Gd/Yb}]_{\text{N}} = 0.5$ –2.8) (Fig. 5a). Their primitive mantle-normalized trace-element distribution patterns are characterized by the enrichment of large ion lithophile elements (LILEs) and the depletion of high field strength elements (HFSEs) (Fig. 5b). All the samples exhibit strong negative Ta–Nb–Ti anomalies (e.g., $[\text{Nb/La}]_{\text{N}} = 0.06$ –0.60) and negative to slightly positive Sr anomalies (Fig. 5b).

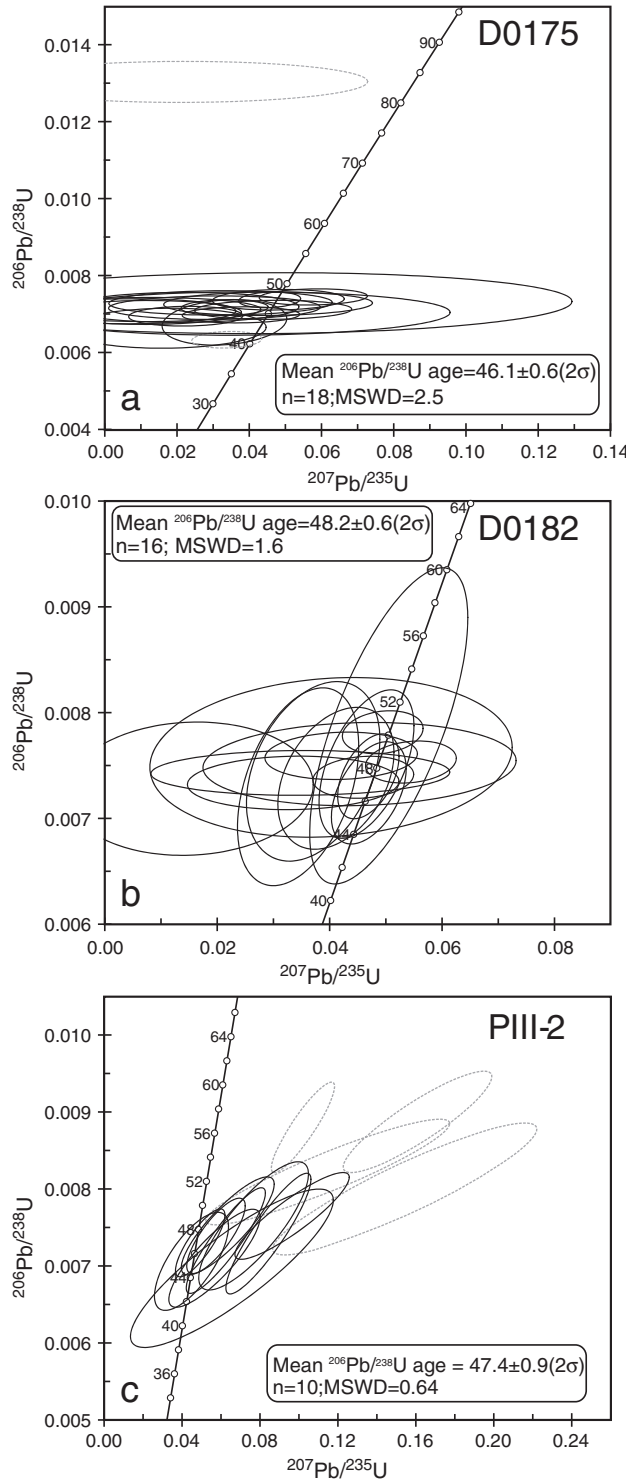


Fig. 3. (a–b) SHRIMP and (c) LA-ICP-MS zircon U-Pb concordia diagrams for the Napuri intrusive rocks in southern Tibet. Dashed and solid line ellipses show the age data with 1 σ errors of inherited and magmatic zircon, respectively.

Based on their REE, Sr and Y contents, the Napuri samples can be divided into three compositional groups. Group I samples (PIII-17 and D0175) show the lowest total REE (55.5–63.2 ppm), especially in HREE (Yb = 0.46–0.48 ppm and Y = 3.56–3.73 ppm), and the highest Sr/Y (77.5–81.3) ratios with obvious positive Eu ($\text{Eu}/\text{Eu}^* = (\text{EuN}/\sqrt[3]{\text{SmN}} \times \text{GdN}) = 1.40–1.43$) and Sr anomalies (Fig. 5a and b). In addition, they show obvious negative Nb anomalies ($(\text{Nb}/\text{La})_N = 0.22–0.25$) (Fig. 5b), and relatively high SiO_2 (70.3–73.9 wt.%) contents

and intermediate Sr (~289 ppm) and $\text{Mg}^\#$ ($(\text{Mg}^{2+}/(\text{Fe}^{2+} + \text{Mg}^{2+})) \times 100 = 44.5–45.4$) values (Table 3). Group II samples have higher Sr (273–718 ppm) contents and total REE (115–375 ppm) contents with negligible to slightly negative Eu ($\text{Eu}/\text{Eu}^* = 0.62–0.88$) and Sr anomalies, and intermediate Y (8.8–16.2 ppm), Yb (0.93–1.77 ppm) and Sr/Y (18.3–65.7) values (Fig. 5). Group III samples (PIII-1 and PIII-2) are characterized by the highest SiO_2 (74.5–76.0 wt.%), Y (17.0–23.7 ppm) and Yb (2.9–3.3 ppm) and lowest Al_2O_3 (12.5–13.2 wt.%) and Sr (81–141 ppm) contents, the lowest Sr/Y (4.8–5.9) ratios, and negative Eu ($\text{Eu}/\text{Eu}^* = 0.40–0.43$) and Sr anomalies (Fig. 5) (Table 3). Their variable $\text{Mg}^\#$ (36.4–62.8) values result from low and variable MgO (0.29–0.69 wt.%) and FeO (0.95–1.18 wt.%) contents (Table 3).

Group I and II rocks display adakitic affinities as defined by Defant and Drummond (1990) (Fig. 6; Table 3), such as low concentrations of HREEs and Y, and high Sr contents and Sr/Y and La/Yb ratios (Figs. 5 and 6). In addition, these samples also show low $\text{Mg}^\#$ values ranging from 36.4 to 49.6, similar to those ($\text{Mg}^\# < 50$) of adakitic rocks derived by partial melting of the mafic lower crust (e.g., Atherton and Petford, 1993; Wang et al., 2007).

4.4. Sr-Nd-Hf isotope geochemistry

Initial isotopic ratios of the Napuri rocks were calculated based on the mean formation age of 48 Ma, and the whole rock Sr-Nd and zircon Hf isotopic composition data are given in Tables 4 and 5, respectively. The three groups of samples exhibit slightly high and variable initial $^{87}\text{Sr}/^{86}\text{Sr}$ isotopic ratios (0.7050–0.7058) and uniform $\varepsilon_{\text{Nd}}(t)$ values (−0.26 to +0.71, average +0.22) with Nd-isotope model ages (T_{DM}) ranging from 0.66 to 0.78 Ga (Table 4). Their Nd-Sr isotope compositions are relatively more enriched than those of the Late Cretaceous Gangdese adakitic rocks derived from the melting of the thickened lower crust (e.g., Guan et al., 2010; Wen et al., 2008b) (Fig. 6a). However, their $\varepsilon_{\text{Nd}}(t)$ values are relatively high compared to those of the Oligocene–Miocene adakitic rocks in southern Tibet (e.g., Chung et al., 2003; Guo et al., 2007; Hou et al., 2004).

The Napuri rocks have relatively low and variable $\varepsilon_{\text{Hf}}(t)_{\text{zircon}}$ values (+3.6 ± 11.4) and positive $\Delta\varepsilon_{\text{Hf}}(t)$ values (+1.5 to +9.1) [where $\Delta\varepsilon_{\text{Hf}}(t) = \varepsilon_{\text{Hf}}(t) - (1.59\varepsilon_{\text{Nd}}(t) + 1.28)$] and plot close to or above the mantle array [$\varepsilon_{\text{Hf}}(t) = 1.59\varepsilon_{\text{Nd}}(t) + 1.28$] of Chauvel et al. (2008) on the $\varepsilon_{\text{Hf}}(t)$ versus $\varepsilon_{\text{Nd}}(t)$ diagram (Fig. 7b). They have Nd-Hf isotopic compositions transitional between the Late Cretaceous slab-derived adakites and the Oligocene–Miocene adakitic rocks in southern Tibet (Fig. 7; Ma et al., 2013a). In addition, the Napuri adakitic rocks also show relatively low $\varepsilon_{\text{Hf}}(t)_{\text{zircon}}$ (+3.6 ± 11.4) compared to those (+9.7 ± 15.1) of the Late Cretaceous, thickened crust-derived, adakitic rocks (Guan et al., 2010). The three groups of samples display similar Sr-Nd-Hf isotopic composition, indicating that they were possibly derived from a common magmatic source (Fig. 7).

5. Discussion

5.1. Petrogenesis

5.1.1. Adakitic (Groups I and II) rocks

As mentioned above, Group I and Group II rocks of the Napuri rocks have adakitic affinities. They were emplaced in the Early Eocene (ca. 48 Ma), and approximately contemporaneous with the reported Early Eocene (ca. 51 Ma) adakitic rocks in the Quxu and Nyingchi areas (Ji et al., 2012; Zhang et al., 2010a). Adakitic rocks may be generated by a variety of mechanisms (Castillo, 2012), such as melting of subducted young and hot oceanic crust (Defant and Drummond, 1990), partial melting of thickened basaltic lower crust (Atherton and Petford, 1993; Chung et al., 2003; Wang et al., 2005), partial melting of subducted continental crust (Wang et al., 2008), crustal assimilation and low-pressure fractional crystallization from parental basaltic magmas (Castillo et al., 1999), high-pressure crystallization (involving

Table 2

Chemical compositions of representative minerals of the Napuri granitoids.

Mineral	Spot number	SiO ₂	TiO ₂	Al ₂ O ₃	Cr ₂ O ₃	FeO	MnO	MgO	CaO	Na ₂ O	K ₂ O	NiO	Total	An	Ab	Or
Plagioclase	08@PIII-16	62.26	—	22.80	—	0.17	—	—	4.58	9.57	0.20	—	99.57	20.7	78.3	1.07
	09@PIII-16	61.17	0.07	23.12	0.02	0.18	—	—	5.25	9.21	0.30	—	99.30	23.6	74.9	1.59
	10@PIII-01	64.53	0.02	21.49	—	0.16	0.01	—	3.88	10.34	0.35	—	100.77	16.9	81.3	1.80
	09@PIII-01	61.18	—	23.21	—	0.21	0.03	0.01	5.71	8.74	0.57	—	99.64	25.7	71.3	3.05
	08@PIII-01	59.20	—	24.98	—	0.23	0.02	—	7.63	7.57	0.37	—	99.99	35.1	62.9	2.01
	02@PIII-01	66.39	0.01	20.24	—	0.04	—	—	1.34	11.49	0.30	—	99.81	5.95	92.5	1.58
	05@PIII-01	68.31	0.04	20.03	0.07	0.01	0.01	0.01	0.29	12.09	0.08	0.03	100.97	1.32	98.3	0.41
Potassium feldspar	05@D0175	66.12	0.02	17.00	—	0.04	—	0.01	0.00	0.31	17.01	0.03	100.52	0.00	2.67	97.3
	06@D0175	63.37	0.13	18.01	0.04	0.09	—	—	0.03	0.95	17.17	0.04	99.82	0.13	7.74	92.1
Sphene	01@PIII-01	29.78	36.75	1.31	—	1.28	0.17	0.01	30.11	—	0.00	0.01	99.41	—	—	—
	01@PIII-16	27.91	35.33	1.25	—	2.18	0.16	0.02	28.18	0.01	0.01	0.01	95.05	—	—	—
	10@PIII-16	28.73	37.01	0.83	0.00	1.44	0.14	—	28.42	0.01	0.01	0.02	96.60	—	—	—
Biotite	08@D0175	37.50	2.33	13.83	0.04	19.53	0.54	11.30	0.05	0.12	10.60	—	95.82	—	—	—
	09@D0175	36.91	2.17	14.25	0.01	19.53	0.51	11.08	0.03	0.17	10.08	0.04	94.77	—	—	—
Magnetite	10@D0175	0.13	—	0.04	0.05	94.72	0.05	—	—	0.09	—	—	95.07	—	—	—

garnet) of mafic magmas derived from mantle wedge peridotites (Macpherson et al., 2006), magma mixing between felsic and basaltic magmas (Streck et al., 2007), and partial melting of tonalitic to granodioritic crust (Kamei et al., 2009). We evaluate these alternative processes

in the following sections with specific reference to the Napuri adakitic rocks.

First, the Sr and Nd isotopic compositions of the Napuri adakitic rocks differ markedly from those of the Neo-Tethyan ophiolites from

Table 3

Major (wt.%) and trace element (ppm) data for the Napuri granitoids. (Watson and Harrison, 1983).

Sample	PIII-17	D0175	PIII-03	PIII-04	PIII-05	PIII-06	PIII-07	PIII-08	PIII-16	D0182	PIII-01	PIII-02	
Group	Group I	Group II	Group II										Group III
SiO ₂	70.29	73.87	72.40	70.69	71.26	71.80	72.32	69.95	68.58	66.37	75.95	74.51	
TiO ₂	0.41	0.17	0.38	0.29	0.30	0.35	0.26	0.47	0.42	0.43	0.17	0.34	
Al ₂ O ₃	15.29	14.01	14.17	15.99	14.93	14.57	14.45	14.70	15.64	17.39	12.47	13.22	
Fe ₂ O ₃ *	1.94	1.12	1.89	1.44	1.66	1.77	1.66	2.68	2.60	2.59	1.18	0.95	
MnO	0.05	0.02	0.05	0.05	0.05	0.05	0.05	0.05	0.05	0.06	0.04	0.04	
MgO	0.67	0.40	0.66	0.61	0.60	0.64	0.54	1.03	1.03	0.94	0.29	0.69	
CaO	1.61	1.16	1.55	1.42	1.45	1.56	1.36	2.39	2.52	2.91	0.82	1.36	
Na ₂ O	4.16	3.52	3.80	3.77	3.89	3.95	3.89	3.80	3.91	4.82	3.22	4.21	
K ₂ O	4.90	5.26	4.40	5.07	5.20	4.58	4.77	4.28	4.66	3.86	5.01	3.58	
P ₂ O ₅	0.05	0.03	0.04	0.05	0.04	0.05	0.04	0.11	0.06	0.06	0.03	0.06	
LOI	0.27	0.14	0.31	0.30	0.27	0.34	0.32	0.24	0.22	0.23	0.52	0.68	
Total	99.65	99.70	99.67	99.65	99.66	99.66	99.70	99.70	99.66	99.69	99.65	99.65	
Mg [#]	44.51	45.42	45.01	49.57	45.94	45.64	43.39	47.25	48.00	45.80	36.42	62.80	
Cr	3.16	2.94	2.89	4.50	3.57	3.19	3.32	6.50	4.33	7.41	1.13	2.69	
Ni	2.16	2.14	2.40	2.26	1.84	1.84	1.58	3.59	3.02	4.47	0.880	2.20	
Rb	77.9	78.5	102	114	109	101	109	99.0	81.7	95.8	192	155	
Sr	289	289	307	346	292	296	273	528	718	498	81.3	141	
Y	3.73	3.56	15.2	14.0	11.2	16.2	9.61	8.81	10.9	15.3	17.0	23.7	
Zr	81.8	84.5	84.8	98.1	119	94.9	83.2	118	59.7	103	106	150	
Nb	3.26	3.20	10.8	10.3	8.64	11.6	9.58	10.5	10.0	9.10	13.6	14.4	
Ba	812	776	702	903	902	726	599	649	1209	1348	141	248	
La	14.4	12.3	31.2	51.9	22.7	30.5	157	36.4	31.9	46.7	25.4	23.0	
Ce	28.3	24.6	68.0	86.0	49.6	67.7	168	70.3	68.3	85.8	42.0	51.9	
Pr	3.3	2.87	8.92	8.89	6.51	9.05	11.1	7.78	8.83	9.71	4.19	7.05	
Nd	11.7	10.4	32.1	29.4	23.0	32.4	27.5	27.1	32.1	34.5	12.5	26.1	
Sm	1.71	1.61	5.27	4.53	3.74	5.19	3.27	4.14	4.98	5.70	1.93	4.94	
Eu	0.630	0.600	0.910	0.890	0.780	0.910	0.700	1.00	1.13	1.24	0.270	0.580	
Gd	1.08	1.07	3.69	3.42	2.76	3.93	2.68	2.90	3.47	4.14	1.88	3.99	
Tb	0.150	0.140	0.560	0.500	0.420	0.580	0.330	0.360	0.430	0.590	0.370	0.690	
Dy	0.790	0.750	3.05	2.76	2.25	3.21	1.75	1.86	2.25	3.30	2.45	4.21	
Ho	0.150	0.140	0.590	0.550	0.440	0.640	0.370	0.350	0.400	0.630	0.610	0.900	
Er	0.400	0.410	1.63	1.55	1.27	1.74	1.04	0.920	1.09	1.71	1.97	2.73	
Tm	0.0700	0.0700	0.250	0.240	0.190	0.270	0.160	0.130	0.160	0.250	0.370	0.470	
Yb	0.480	0.460	1.67	1.53	1.31	1.77	1.13	0.930	1.04	1.63	2.91	3.30	
Lu	0.0800	0.0800	0.250	0.240	0.200	0.270	0.180	0.160	0.160	0.250	0.520	0.550	
Hf	2.33	2.42	2.81	3.03	3.51	2.97	2.93	3.63	1.77	3.00	4.10	5.16	
Ta	0.410	0.390	1.11	1.05	0.850	1.13	0.960	0.900	0.890	0.960	1.76	2.02	
Pb	15.0	14.4	16.2	16.6	15.7	15.2	16.8	21.4	23.8	13.3	15.5	12.4	
Th	4.14	4.02	8.18	13.7	24.6	9.93	58.5	16.9	6.93	12.4	35.9	34.3	
U	0.800	0.910	1.97	1.97	3.06	1.73	6.65	4.47	1.52	2.63	6.41	4.97	
La/Yb	29.9	27.0	18.7	33.9	17.3	17.3	140	39.2	30.6	28.6	8.73	6.96	
Sr/Y	77.5	81.3	20.2	24.7	26.1	18.3	28.4	60.0	65.7	32.5	4.79	5.92	
(La/Yb) _N	21.4	19.3	13.4	24.3	12.4	100	28.1	22.0	20.5	6.26	5.00		
T _{Zr}	724	733	731	748	755	739	730	748	694	734	754	778	

Fe₂O₃*: Total Fe₂O₃; LOI: Loss on Ignition; Mg[#]: Mg²⁺/(Mg²⁺ + Mg²⁺) × 100; T_{Zr}: Zircon saturation temperature.

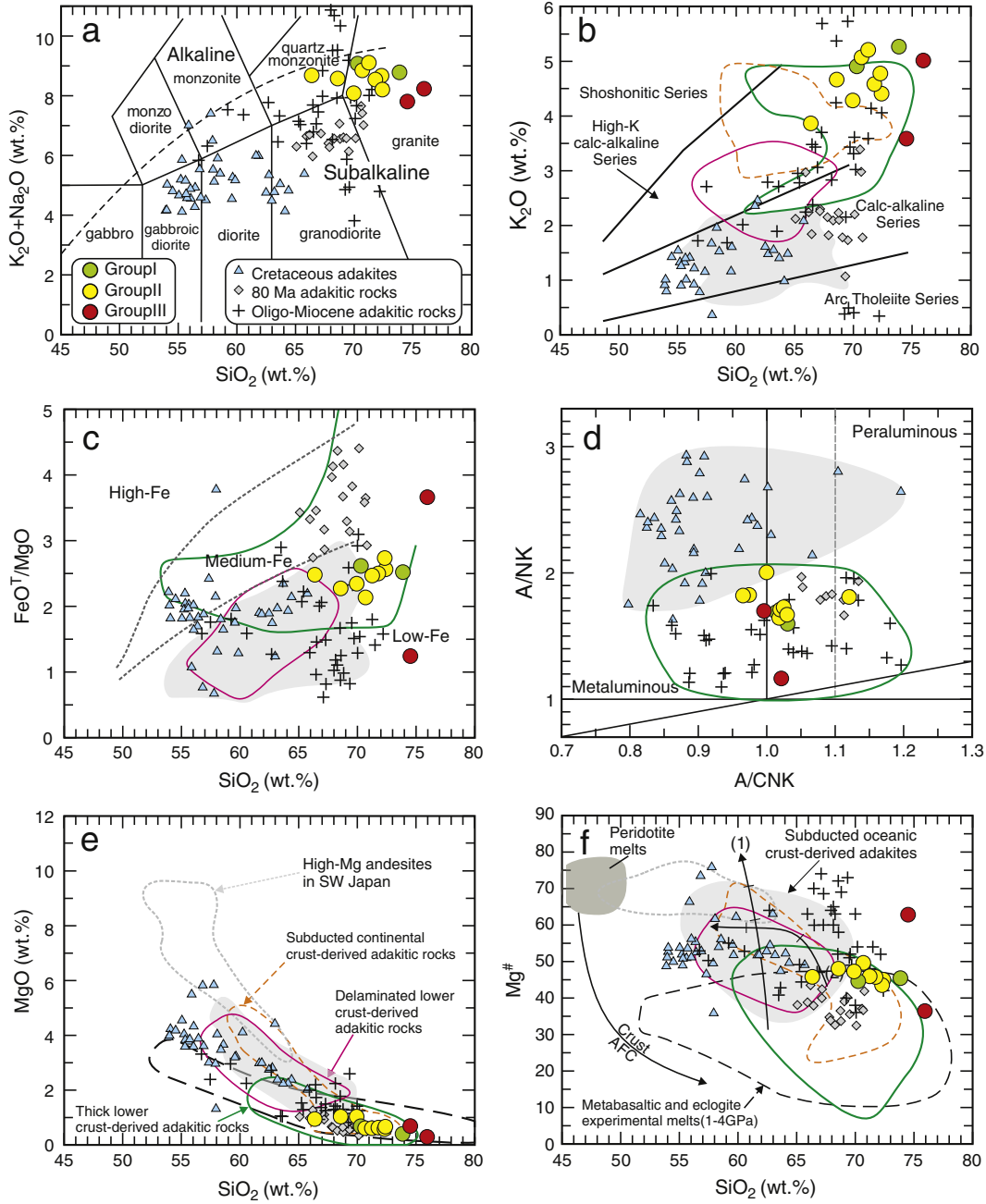


Fig. 4. (a) SiO_2 versus $\text{K}_2\text{O} + \text{Na}_2\text{O}$ plot (Middlemost, 1994). (b) SiO_2 versus K_2O plot (Peccerillo and Taylor, 1976). (c) SiO_2 versus FeO^T/MgO diagrams (Miyashiro, 1974). Boundaries (grey lines) between low-, medium-, and high-Fe suites are after Arculus (2003). (d) A/NK versus A/CNK diagram (Maniar and Piccoli, 1989); (e) SiO_2 versus MgO diagram. (f) SiO_2 versus $\text{Mg}^\#$ diagram. Mantle AFC curves, with proportions of assimilated peridotite indicated, are after Stern and Kilian (1996) (Curve 1) and Rapp et al. (1999) (Curve 2), peridotite melts and crust AFC curves from Stern and Kilian (1996). Data for metabasalt and eclogite experimental melts (1–4.0 GPa), and peridotite-hybridized equivalents, are from Rapp et al. (1999) and references therein. Data for high-Mg andesites of SW Japan are from the following references: Shimoda et al. (1998), and Tatsumi (2006) and references therein. Data for the Cretaceous adakitic rocks are from Jiang et al. (2012), Ma et al. (2013a), Zhang et al. (2010b) and Zhu et al. (2009). Data for the 80 Ma adakitic rocks are from Wen et al. (2008a) and Guan et al. (2010). Data for the Oligo-Miocene adakitic rocks are from Chung et al. (2003), Gao et al. (2007), Guan et al. (2012), Guo et al. (2007), Hou et al. (2004), Jiang et al. (2011), Xu et al. (2010) and Zhang et al. (2010a). The fields of subducted oceanic crust-, delaminated lower crust-, and thickened lower crust-derived adakites are after Wang et al. (2006).

the IYTS (Fig. 7a; Xu and Castillo, 2004), thus precluding the possibility that they were derived from the subducted Neo-Tethyan oceanic crust (Fig. 7a). Moreover, their low $\text{Mg}^\#$ (36.4–49.6) values and Ni (0.8–4.5 ppm) and Cr (<7.4 ppm) contents are distinct from those ($\text{Mg}^\# > 47$; Ni = 20–40 ppm and Cr = 30–50 ppm) of the subducted oceanic slab-derived adakites (Martin, 1999).

Second, they could not have been generated by melting of an upper mantle source metasomatized by slab-released melts in the Neo-

Tethyan subduction as proposed by Gao et al. (2007, 2010) for the Oligo-Miocene adakitic rocks in southern Lhasa. Chung et al. (2009) suggested that mantle sources were unlikely, given that there are no mantle-derived mafic rocks associated with the Oligo-Miocene adakitic rocks. Although the Napuri adakitic magmas are contemporary with the Gangdese peak activities at ca. 50 Ma (e.g., Ji et al., 2009; Lee et al., 2009, 2012; Wen et al., 2008a), their higher SiO_2 (66.4–73.9 wt.%) and lower MgO (0.4–1.0 wt.%) and compatible element (Cr = 2.9–7.4 ppm;

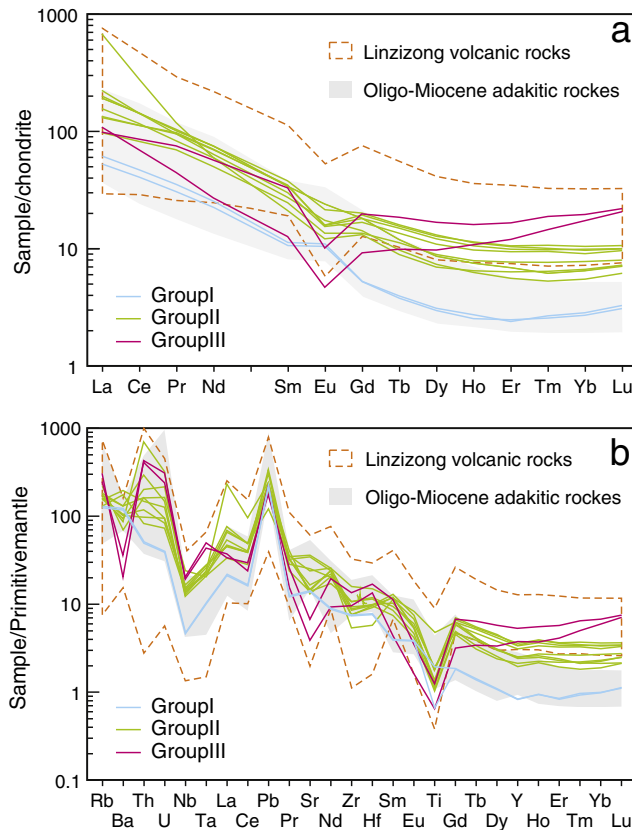


Fig. 5. (a) Chondrite-normalized rare earth element (REE) patterns and (b) primitive mantle-normalized multi-element patterns of the Napuri granitoids. Data for the Linzizong volcanic rocks are from Lee et al. (2012) and Mo et al. (2007). The Oligo-Miocene adakites data are from Chung et al. (2003), Guo et al. (2007) and Hou et al. (2004). The chondrite and primitive mantle normalization values are from Sun and McDonough (1989).

Ni = 1.6–4.5 ppm) contents also do not accord with a mantle origin (Martin et al., 2005). Their relatively enriched Sr-Nd isotopic compositions also argue against such a source (Fig. 7a).

Third, the relatively high $\epsilon_{\text{Nd}}(t)$ and positive zircon $\epsilon_{\text{Hf}}(t)$ values ($\epsilon_{\text{Nd}}(t) = +0.27$ to $+0.71$; $\epsilon_{\text{Hf}}(t)_{\text{zircon}} = +3.6$ to $+11.4$) of the Napuri adakitic rocks do not match the geochemical features ($\epsilon_{\text{Nd}}(t) \leq 3$) of adakitic rocks derived from subducted continental crust (Wang et al.,

2008). The Napuri samples are also characterized by higher SiO₂ and lower MgO and compatible element contents (Table 3) than subducted continental crust-derived adakitic magmas (SiO₂: 55–69 wt.%; MgO: 1.4–6.3 wt.%) that generally undergo interaction with the mantle wedge peridotite during magma ascent (Wang et al., 2008).

Fourth, Group I and Group II adakitic rocks could not have been generated by high- or low-pressure crystallization from basaltic parental magmas. Given that high-pressure crystallization involving garnet will cause a decrease in HREE and Y contents, the Sr/Y and Dy/Yb ratios of residual magmas will increase with increasing SiO₂ contents (Macpherson et al., 2006). However, the Napuri adakitic rocks do not show such trends in their chondrite-normalized rare earth element patterns (Fig. 6a) or on Dy/Yb, (La/Yb)_N and Sr/Y versus SiO₂ diagrams (Fig. 8d–f). The Group I samples display obvious positive Eu and Sr anomalies (Fig. 5), indicating that fractional crystallization of plagioclase did not play an important role in their formation. In contrast, the Group II samples show negligible or slightly negative Eu and Sr anomalies (Fig. 5a), which may possibly be produced by fractional crystallization of a substantial amount of plagioclase (e.g., Bédard, 2006; Bindeman and Davis, 2000) or the occurrence of some residual plagioclase in the magmatic source. However, the similar or higher Al₂O₃ and Sr contents of Group II rocks suggest that they could not have been generated by fractional crystallization of plagioclase from magmas compositionally similar to Group I rocks. On the other hand, amphibole generally favors middle and to a lesser extent HREE relative to LREE (e.g., Brenan et al., 1995). However, as indicated by the preservation of a strong positive correlation between (Dy/Yb)_N and (La/Yb)_N (Fig. 9a), fractional crystallization of amphibole was not a significant process for most Napuri samples. The amount of amphibole that can be formed is limited by the Fe and Mg budget to a small mass fraction (in the region of 20%), strongly reducing its potential effect (Moyen, 2009). The low Fe₂O₃* (total Fe₂O₃) and MgO contents of the Napuri rocks do not support significant fractional crystallization of amphibole. In summary, fractional crystallization of amphibole and plagioclase was not responsible for the adakitic affinities of the Napuri Group I and Group II samples.

Fifth, it is unlikely that magma mixing between felsic and basaltic magmas can account for the Napuri adakitic rocks. Magma mixing generally requires mantle-derived basaltic and crust-derived felsic end-members (e.g., Streck et al., 2007). In southern Lhasa, the candidates for mantle-derived basaltic and crust-derived felsic end-members are most plausibly represented by the 65–40 Ma Linzizong mafic magmas (e.g., Lee et al., 2012; Mo et al., 2007) and the synchronous (45–53 Ma) Gangdese granites (e.g., Ji et al., 2009, 2012; Wen et al., 2008a), respectively. However, the $\epsilon_{\text{Nd}}(t)$ and $\epsilon_{\text{Hf}}(t)$ values of the Napuri adakitic rocks are lower than those of both the felsic and basaltic end-members,

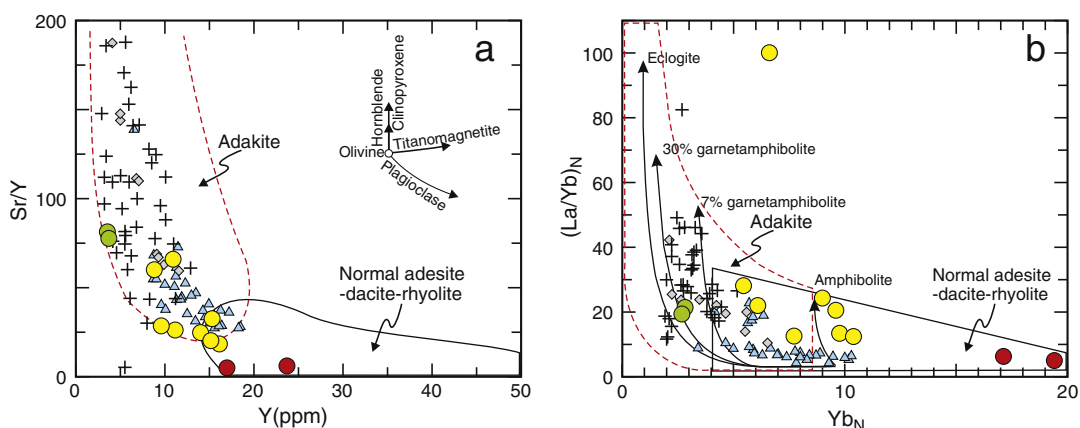


Fig. 6. (a) Y versus Sr/Y diagram and (b) Yb_N versus (La/Yb)_N diagram for the Napuri intrusive rocks. Fields of adakite and arc magmatic rocks are from Defant and Drummond (1990) and Petford and Atherton (1996). Crystal fractionation paths of the primary minerals are from Castillo et al. (1999). N denotes normalized to chondrite composition (Sun and McDonough, 1989). Data sources and symbols are the same as for Fig. 4.

Table 4

Sr and Nd isotope data for the Napuri granitoids.

Sample	Group	$^{87}\text{Rb}/^{86}\text{Sr}$	$^{87}\text{Sr}/^{86}\text{Sr} \pm 2\sigma$	$(^{87}\text{Sr}/^{86}\text{Sr})_i$	$^{147}\text{Sm}/^{144}\text{Nd}$	$^{143}\text{Nd}/^{144}\text{Nd} \pm 2\sigma$	$(^{143}\text{Nd}/^{144}\text{Nd})_i$	$\epsilon_{\text{Nd}}(t)$	T_{DM} (Ma)
PIII-17	I	0.7794	0.706023 \pm 8	0.7055	0.0885	0.512605 \pm 7	0.5126	0.01	667
D0175	I	0.7840	0.705591 \pm 6	0.7051	0.0940	0.512629 \pm 7	0.5126	0.44	668
PIII-04	II	0.9565	0.705653 \pm 9	0.7050	0.0933	0.512593 \pm 7	0.5126	-0.27	710
PIII-05	II	1.079	0.765645 \pm 8	0.7649	0.0980	0.512614 \pm 9	0.5126	0.11	711
PIII-08	II	0.5419	0.705848 \pm 7	0.7055	0.0921	0.512600 \pm 8	0.5126	-0.11	693
PIII-16	II	0.3287	0.705421 \pm 9	0.7052	0.0937	0.512633 \pm 6	0.5126	0.52	661
D0182	II	0.5563	0.705473 \pm 11	0.7051	0.0999	0.512607 \pm 7	0.5126	-0.02	732
PIII-01	III	6.830	0.709819 \pm 7	0.7053	0.0931	0.512636 \pm 9	0.5126	0.58	654
PIII-02	III	3.196	0.707380 \pm 9	0.7053	0.1143	0.512649 \pm 7	0.5126	0.71	775

 $^{87}\text{Rb}/^{86}\text{Sr}$ and $^{147}\text{Sm}/^{144}\text{Nd}$ are calculated using whole-rock Rb, Sr, Sm and Nd contents in Table 3.
 $\epsilon_{\text{Nd}}(t) = [(^{143}\text{Nd}/^{144}\text{Nd})_{\text{sample}}/(^{143}\text{Nd}/^{144}\text{Nd})_{\text{CHUR}} - 1] \times 10,000$. $T_{\text{DM}} = \ln[(^{143}\text{Nd}/^{144}\text{Nd})_{\text{sample}} - (^{143}\text{Nd}/^{144}\text{Nd})_{\text{DM}}]/[(^{143}\text{Sm}/^{144}\text{Nd})_{\text{sample}} - (^{143}\text{Sm}/^{144}\text{Nd})_{\text{DM}}]/\lambda$ (DePaolo, 1988). In the calculation, $(^{143}\text{Nd}/^{144}\text{Nd})_{\text{CHUR}} = 0.512638$, $(^{147}\text{Sm}/^{144}\text{Nd})_{\text{CHUR}} = 0.1967$, $(^{143}\text{Nd}/^{144}\text{Nd})_{\text{DM}} = 0 \cdot 51,315$, $(^{147}\text{Sm}/^{144}\text{Nd})_{\text{DM}} = 0 \cdot 2136$ and $t = 48$ Ma.

and the lack of corresponding changes in $\epsilon_{\text{Nd}}(t)$ and $(^{87}\text{Sr}/^{86}\text{Sr})_i$ values with increasing SiO_2 and $^{147}\text{Sm}/^{144}\text{Nd}$ values (Fig. 8g–i), are inconsistent with the magma mixing model (e.g., Streck et al., 2007).

Finally, the Napuri adakitic rocks are also unlikely to have been produced by melting of the Gangdese Jurassic–Eocene granitoids as proposed by Pan et al. (2012) and Zhang et al. (2010a). Adakitic rocks

derived from partial melting of granodioritic crust, as reported by Kamei et al. (2009), should be peraluminous, which is inconsistent with the features of the Napuri adakitic rocks (Fig. 4d). In addition, the relatively low $\epsilon_{\text{Nd}}(t)$ and $\epsilon_{\text{Hf}}(t)$ isotopic values of the Napuri adakitic rocks compared to Gangdese Jurassic–Eocene granitoids (e.g., Ji et al., 2009, 2012; Wen et al., 2008a) further rules out this possibility. The

Table 5

Zircon Hf isotope data for the Napuri granitoids.

Spot number	$^{176}\text{Yb}/^{177}\text{Hf}$	2σ	$^{176}\text{Lu}/^{177}\text{Hf}$	2σ	$^{176}\text{Hf}/^{177}\text{Hf}$	2σ	$\epsilon_{\text{Hf}}(t)$	2σ	T_{DM} (Ma)
PIII-2 (1)	0.043615	0.000737	0.001819	0.000020	0.282963	0.000025	7.7	0.9	418
PIII-2 (2)	0.043063	0.000880	0.001810	0.000036	0.283011	0.000028	9.7	1.0	348
PIII-2 (3)	0.097662	0.003056	0.004119	0.000125	0.282981	0.000024	8.9	0.9	419
PIII-2 (4)	0.071793	0.003759	0.002823	0.000136	0.283016	0.000031	9.6	1.1	351
PIII-2 (5)	0.043170	0.000569	0.001972	0.000041	0.282946	0.000030	7.5	1.1	445
PIII-2 (6)	0.054974	0.002284	0.002261	0.000081	0.282937	0.000032	6.8	1.1	462
PIII-2 (7)	0.043352	0.000212	0.001798	0.000009	0.282968	0.000023	8.1	0.8	411
PIII-2 (8)	0.058069	0.000673	0.002315	0.000023	0.282909	0.000019	5.8	0.7	504
PIII-2 (9)	0.046506	0.001309	0.001992	0.000038	0.282853	0.000052	3.9	1.8	581
PIII-2 (10)	0.038997	0.000600	0.001596	0.000022	0.282935	0.000029	6.7	1.0	456
PIII-2 (11)	0.050217	0.000834	0.002049	0.000031	0.283031	0.000032	10.1	1.1	322
PIII-2 (12)	0.045445	0.001610	0.001886	0.000057	0.282981	0.000031	8.4	1.1	393
PIII-2 (13)	0.049949	0.001956	0.002028	0.000066	0.28291	0.000028	6.0	1.0	498
PIII-2 (14)	0.076458	0.001864	0.002991	0.000072	0.282991	0.000027	8.7	1.0	390
PIII-2 (15)	0.050989	0.001301	0.002104	0.000048	0.28299	0.000025	8.6	0.9	382
PIII-2 (16)	0.046798	0.000409	0.001872	0.000025	0.282983	0.000025	8.5	0.9	390
D0182 (12)	0.061874	0.002650	0.002396	0.000105	0.283057	0.000028	11.1	1.0	287
D0182 (11)	0.053181	0.000735	0.001908	0.000020	0.282937	0.000026	6.8	0.9	458
D0182 (10)	0.039730	0.000218	0.001595	0.000006	0.282974	0.000021	8.1	0.7	401
D0182 (9)	0.029830	0.000475	0.001209	0.000019	0.282886	0.000025	5.1	0.9	521
D0182 (8)	0.075670	0.000691	0.002928	0.000026	0.282979	0.000023	8.3	0.8	408
D0182 (7)	0.042775	0.000649	0.001763	0.000019	0.283022	0.000026	9.9	0.9	332
D0182 (6)	0.041469	0.000289	0.001555	0.000009	0.282965	0.000026	7.8	0.9	413
D0182 (5)	0.056032	0.001628	0.002388	0.000056	0.282966	0.000025	7.8	0.9	421
D0182 (4)	0.028257	0.000309	0.001065	0.000012	0.282961	0.000021	7.7	0.8	413
D0182 (3)	0.058881	0.000767	0.002304	0.000026	0.283003	0.000030	9.2	1.1	365
D0182 (2)	0.037526	0.000800	0.001464	0.000033	0.282941	0.000029	7.0	1.0	446
D0182 (1)	0.075988	0.000693	0.002585	0.000020	0.282964	0.000030	7.8	1.1	426
D0175 (12)	0.051298	0.000627	0.001856	0.000021	0.282876	0.000027	4.6	1.0	545
D0175 (11)	0.048167	0.000631	0.001870	0.000021	0.282938	0.000029	6.8	1.0	456
D0175 (10)	0.040364	0.000202	0.001590	0.000007	0.282939	0.000024	6.9	0.9	451
D0175 (9)	0.050422	0.000145	0.001973	0.000004	0.282953	0.000020	7.4	0.7	435
D0175 (8)	0.023672	0.000197	0.000861	0.000009	0.283067	0.000024	11.4	0.8	261
D0175 (7)	0.056459	0.000357	0.002124	0.000014	0.282933	0.000020	6.6	0.7	467
D0175 (6)	0.040760	0.000299	0.001494	0.000010	0.282858	0.000023	4.0	0.8	565
D0175 (5)	0.048807	0.000767	0.001811	0.000027	0.282847	0.000024	3.6	0.9	587
D0175 (4)	0.056787	0.000519	0.002135	0.000018	0.282963	0.000020	7.7	0.7	422
D0175 (3)	0.026097	0.000432	0.001104	0.000017	0.282933	0.000023	6.7	0.8	453
D0175 (2)	0.039195	0.000262	0.001431	0.000009	0.282878	0.000021	4.7	0.8	536
D0175 (1)	0.054009	0.001185	0.001938	0.000041	0.283008	0.000020	9.3	0.7	355

 $\epsilon_{\text{Hf}}(t) = [^{176}\text{Hf}/^{177}\text{Hf}_Z/^{176}\text{Hf}/^{177}\text{Hf}_{\text{CHUR}}(t) - 1] \times 10,000$; $^{176}\text{Hf}/^{177}\text{Hf}_{\text{CHUR}}(t) = ^{176}\text{Hf}/^{177}\text{Hf}_{\text{CHUR}}(0) - ^{176}\text{Lu}/^{177}\text{Hf}_{\text{CHUR}} \times (e^{kt} - 1)$. $T_{\text{DM}} = (1/\lambda) \times \ln[1 + (^{176}\text{Hf}/^{177}\text{Hf}_{\text{DM}} - ^{176}\text{Hf}/^{177}\text{Hf}_Z)/(^{176}\text{Lu}/^{177}\text{Hf}_{\text{DM}} - ^{176}\text{Lu}/^{177}\text{Hf}_Z)]$; where f_{Hf}^C , f_{Hf} zircon and f_{Hf} DM are the $f_{\text{Lu/Hf}}$ values of the continental crust, zircon sample and the depleted mantle; subscript Z = analyzed zircon sample, CHUR = chondritic uniform reservoir; DM = depleted mantle; T = 48 Ma, mean age of the Napuri granitoids; $\lambda = 1.867 \times 10^{-11}$ year $^{-1}$, decay constant of ^{176}Lu (Soderlund et al., 2004); $^{176}\text{Hf}/^{177}\text{Hf}_{\text{DM}} = 0.28325$; $^{176}\text{Lu}/^{177}\text{Hf}_{\text{DM}} = 0.0384$; present-day $^{176}\text{Hf}/^{177}\text{Hf}_{\text{CHUR}}(0) = 0.282772$; $^{176}\text{Hf}/^{177}\text{Hf}_{\text{CHUR}} = 0.0332$; $^{176}\text{Hf}/^{177}\text{Hf}_{\text{C}} = 0.015$.

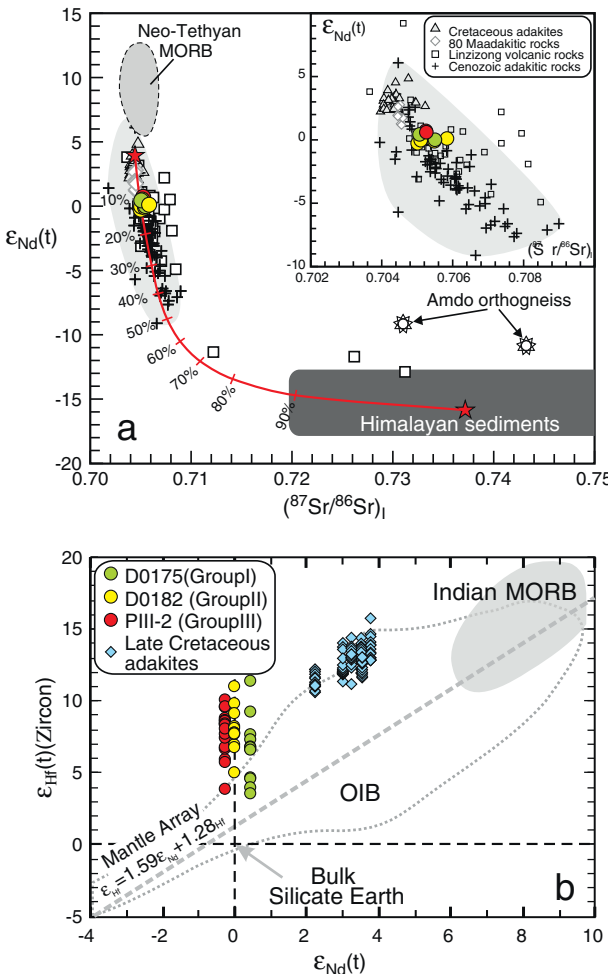


Fig. 7. (a) $\epsilon_{\text{Nd}}(t)$ vs. $(^{87}\text{Sr}/^{86}\text{Sr})_i$ (enlarged diagram in inset); (b) zircon $\epsilon_{\text{Hf}}(t)/\text{Zircon } \epsilon_{\text{Nd}}(t)$ diagrams for the Napuri intrusive rocks. Data sources for (a): Neo-Tethyan middle oceanic ridge basalts (MORB) – the IYTS ophiolites (Xu and Castillo, 2004); Himalayan sediments – Himalayan leucogranites (Guo and Wilson, 2012); Cretaceous adakites (Jiang et al., 2011; Ma et al., 2013a; Zhu et al., 2009); 80 Ma thickened mafic lower crust-derived adakitic rocks (Wen et al., 2008b); the Linzizong volcanic rocks (Lee et al., 2012; Mo et al., 2007); Cenozoic (Oligo-Miocene) adakitic rocks (Gao et al., 2010; Guan et al., 2012; Guo et al., 2007; Hou et al., 2004; Ji et al., 2012; Jiang et al., 2012; Xu et al., 2010; Zhang et al., 2010a); the Amdo orthogneiss (Harris et al., 1988); sample NL-07 (leucogranite, representing the Himalayan sediments ($\text{Nd} = 11.1 \text{ ppm}$, $\epsilon_{\text{Nd}}(t) = 47 \text{ Ma} = -15.9$, $\text{Sr} = 89.0 \text{ ppm}$, $(^{87}\text{Sr}/^{86}\text{Sr})_i = 0.7372$) (Guo and Wilson, 2012). Data sources for (b): Hf isotopic results of Late Cretaceous adakites (Ma et al., 2013a); fields of Hf-Nd isotopic data for Indian Ocean MORB, OIB and mantle array (Chauvel and Blachert-Toft, 2001; Ingle et al., 2003).

Group I samples are also characterized by positive Eu and Sr anomalies, which contradicts a model of partial melting of arc-type tonalites with amphibole and plagioclase as residual phases (Kamei et al., 2009).

In view of the above discussion, and the observation that the high K_2O contents, low MgO , Cr , Ni contents and $\text{Mg}^\#$ values of the Napuri adakitic rocks are similar to those of thickened lower crust-derived adakitic melts (Fig. 4; Atherton and Petford, 1993; Chung et al., 2003; Wang et al., 2007), we suggest that the Napuri adakitic rocks were most probably generated by partial melting of the continental mafic lower crust.

Given that garnet is the only rock-forming mineral that can substantially fractionate middle REE from heavy REE, Huang and He (2010) suggested that high $(\text{Dy/Yb})_\text{N}$ ratios best reveal the involvement of garnet. Moreover, as D_{REE} values increase with atomic numbers, garnet is the only rock-forming mineral that can substantially enhance both $(\text{La/Yb})_\text{N}$ and $(\text{Dy/Yb})_\text{N}$ (or $(\text{Gd/Yb})_\text{N}$) of magmas (e.g., Klein et al., 2000). Thus, the positively correlated high $(\text{Dy/Yb})_\text{N}$ and $(\text{La/Yb})_\text{N}$ ratios (Fig. 9a) suggest a dominant role of garnet in the REE fractionation of the

Napuri samples during partial melting. Experimental studies (e.g., Rapp et al., 2003 and references therein) have also shown that mafic crustal rocks can melt to produce adakitic liquids at sufficient depths (>40 km, i.e., ~1.2 GPa) for garnet to be stable within the residual assemblage (e.g., garnet-amphibolite, amphibole-bearing eclogite and/or eclogite).

Therefore, the Napuri adakitic rocks (Groups I and II) were most likely generated by partial melting of mafic lower crust in the garnet stability field. The Group II samples, however, show higher REE (especially HREEs) and Y contents than Group I and slightly negative Eu anomalies (Fig. 5a). As mentioned above, Group II rocks display similar or higher Al_2O_3 and Sr contents than the Group I rocks and could not have been generated by fractional crystallization of plagioclase from magmas compositionally similar to Group I rocks. Thus, we suggest that the Group I rocks were generated from a magmatic source with residual garnet but no plagioclase (i.e., an eclogitic source), whereas Group II rocks were most probably derived from a magmatic source with residual plagioclase and garnet (i.e., a garnet-amphibolitic source). This implies that the two groups of rocks were derived from crustal source rocks at different depths. The Napuri Group I adakitic rocks were probably derived from lower degree melting of a deeper lower crustal source (an amphibole eclogite), whereas the Group II rocks may have originated from a garnet-amphibolite with higher degrees of melting, consistent with their insignificant negative Eu and Sr anomalies (Fig. 5a; Table 3). In addition, the Napuri Group I rocks have REE and multi-elemental patterns and positive Eu anomalies similar to those of the Oligo-Miocene adakitic rocks in southern Lhasa (Fig. 5), indicating that they may have been derived from similar crustal sources at similar depths.

5.1.2. Group III rocks

The Group III rocks are characterized by the highest SiO_2 (74.5–76.0 wt.%) and HREE contents and the lowest $(\text{La/Yb})_\text{N}$ (5.0–6.3) and Sr/Y (4.8–5.9) ratios with significant negative Eu and Sr anomalies (Fig. 5), which are obviously different from the Group I and Group II adakites (Figs. 5 and 6). Although the Group III rocks have geochemical compositions in common with widespread non-adakitic Gangdese granitoids, their association with adakitic rocks, and similar petrographic and outcrop characteristics, suggests that the genesis of Group III rocks probably differed from that of common Eocene Gangdese granitoids. Group III rocks were sampled from the central part of the Napuri intrusion (Fig. 1c). In addition, they display Sr-Nd-Hf isotopic compositions similar to the Group I and Group II rocks (Fig. 7), which also suggests a shared magmatic source. Here, we propose that they were produced by substantial amounts of fractional crystallization of plagioclase from a parental magma similar that of Group I rocks, owing to their higher SiO_2 contents and obvious Eu and Sr anomalies (Fig. 5). A simple fractional crystallization model indicates that melts of Group I rocks could, via ca. 10% plagioclase fractional crystallization, generate the distinctive geochemical characteristics (e.g., low Sr/Y values, negative Eu anomalies and REE pattern) of the Group III rocks (Fig. 9b and c). Moreover, plagioclase crystals with diameters greater than 1 cm in the Napuri rocks also support the possibility of fractional crystallization. Nonetheless, we do not suggest that the common Eocene Gangdese granitoids were generated by such a mechanism.

In summary, the Group I and Group II Napuri adakitic rocks were generated by partial melting of amphibolite eclogites or garnet amphibolites in the garnet stability field (i.e. thickened juvenile continental mafic lower crust), and the Napuri Group III rocks were probably generated by fractional crystallization of plagioclase from amphibolite eclogite- or garnet amphibolite-derived adakitic magmas.

5.2. Slab breakoff and crustal thickening

5.2.1. Early Eocene Neo-Tethyan slab break-off

The Napuri adakitic rocks were emplaced in the Early Eocene (ca. 48 Ma), coinciding with the peak Gangdese magmatic activities at ca. 50 Ma (Chung et al., 2005; Ji et al., 2009, 2012; Lee et al., 2009,

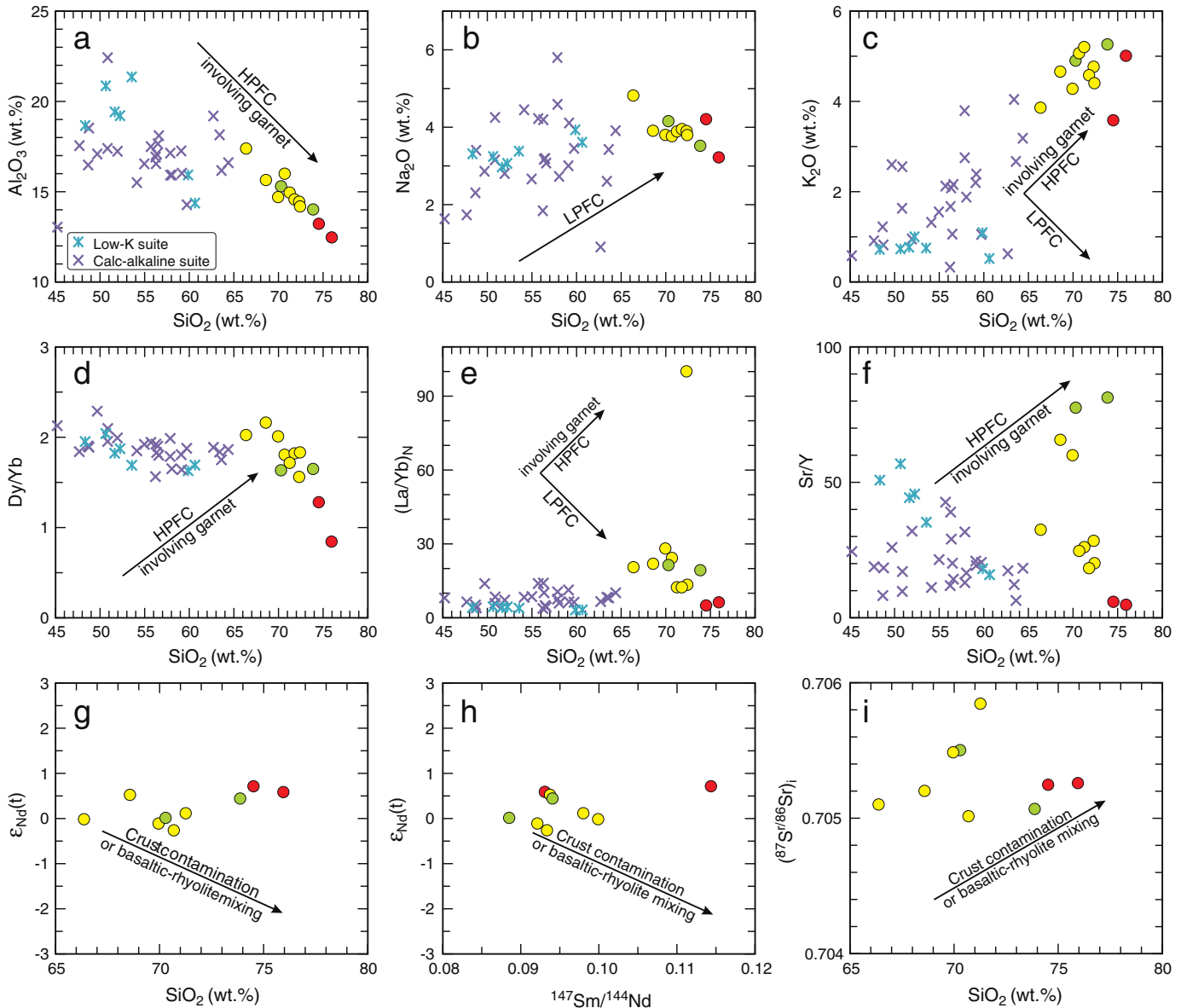


Fig. 8. Plots of (a) SiO_2 versus Al_2O_3 ; (b) SiO_2 versus Na_2O ; (c) SiO_2 versus K_2O ; (d) SiO_2 versus Dy/Yb ; (e) SiO_2 versus $(\text{La}/\text{Yb})_{\text{N}}$; (f) SiO_2 versus Sr/Y ; (g) SiO_2 versus $\epsilon_{\text{Nd}}(t)$; (h) $^{147}\text{Sm}/^{144}\text{Nd}$ versus $\epsilon_{\text{Nd}}(t)$; (i) SiO_2 versus $(^{87}\text{Sr}/^{86}\text{Sr})_i$ for the Napuri intrusive rocks. HPFC, high-pressure fractional crystallization involving garnet (Macpherson et al., 2006); LPFC: crystal fractionation of island arc tholeiitic series basalt (Castillo et al., 1999). Data of the low K suite and calc-alkaline suite from the Pana Group (upper Linzizong Formation) volcanic rocks are from Lee et al. (2012). Data sources and symbols are the same as for Fig. 4.

2012; Wen et al., 2008a). Here we use the slab break-off model to account for both the formation of the Napuri adakitic rocks and the associated magmatic “flare-up” event (e.g., Chung et al., 2005; Ji et al., 2009, 2012; Lee et al., 2009, 2012; Wen et al., 2008a; Zhu et al., 2011).

When two continents collide, the tensile stresses between the buoyant continental lithosphere and previously subducted oceanic lithosphere lead to the separation of the oceanic slab from the continental lithosphere (e.g., Davies and von Blanckenburg, 1995; van Hunen and Allen, 2011; von Blanckenburg and Davis, 1995). Slab break-off typically occurs in the early stages of continental collisions (von Blanckenburg and Davis, 1995), and can place important constraints on associated collision dynamics (van Hunen and Allen, 2011). Timing and other details of the Neo-Tethyan slab break-off in the India–Asia collision belt have long been an issue of hot debate (e.g., Chung et al., 2005; Ji et al., 2009, 2012; Lee et al., 2009, 2012; Wen et al., 2008a; Xu et al., 2008; Zhu et al., 2013). The following lines of evidence support the argument that the Neo-Tethyan slab break-off probably took place in the Early Eocene (ca. 51–46 Ma).

First, slab break-off has an intrinsic preference to start with a narrow slab window between the continent and the subducted oceanic slab, which would result in a linear magmatic belt (Davies and von Blanckenburg, 1995). Previous geochronological investigations indicate that the Paleocene–Eocene Gangdese magmatic intrusive rocks and Linzizong Formation volcanism were synchronous and represent an episode of intense magmatism confined to a narrow zone on the southern margin of the Lhasa block (Fig. 1a; e.g., Ji et al., 2009, 2012; Lee et al., 2009, 2012; Mo et al., 2007; Wen et al., 2008a).

Second, the upwelling of asthenosphere during slab break-off can trigger the formation of a variety of magmas, especially tholeiitic basaltic magma (e.g., von Blanckenburg and Davis, 1995; Xu et al., 2008), which would contribute to the Cenozoic “flare-up” of mafic to felsic arc magmatic rocks in southern Tibet (e.g., Chung et al., 2005; Lee et al., 2009; Mo et al., 2007). For example, low-K tholeiitic basalts, generated by decompression melting of the asthenosphere, have been identified in the Pana Group (the upper Linzizong Formation, ca. 50–43 Ma) (Lee et al., 2012), which is consistent with the slab break-off model. The

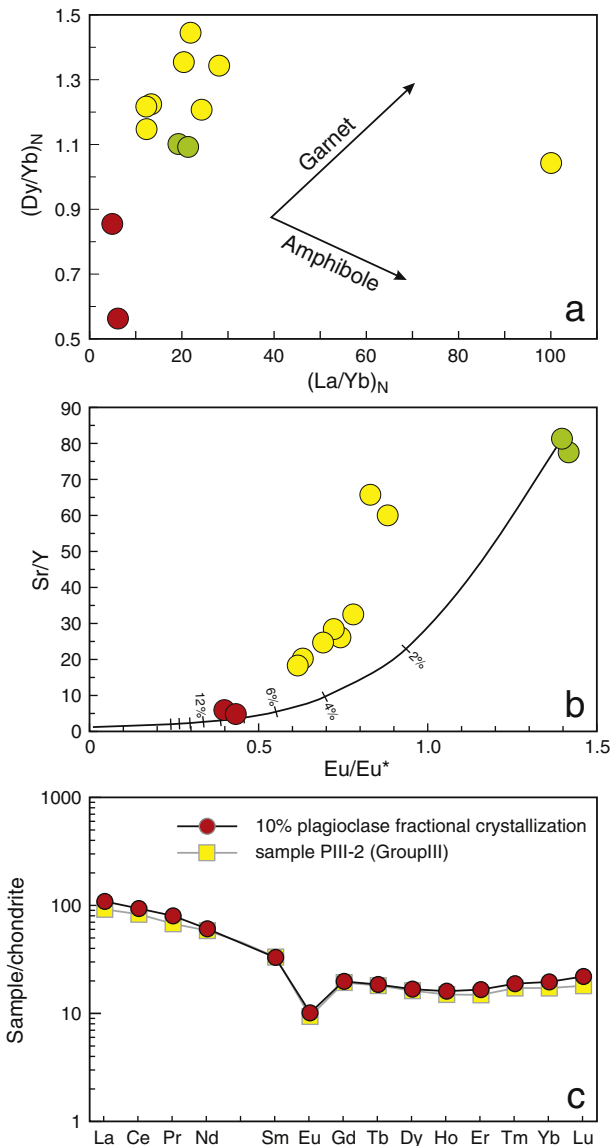


Fig. 9. Plots of (a) $(\text{La}/\text{Yb})_N$ versus $(\text{Dy}/\text{Yb})_N$; (b) Eu/Eu^* versus Sr/Y and (c) chondrite-normalized rare earth element (REE) patterns for Napuri intrusive rocks. Crystal fractionation trend line for garnet and amphibole are after He et al. (2011). The partition coefficient of plagioclase is from McKenzie and O'Nions (1991). Data sources and symbols are the same as for Fig. 4.

detachment of the Neo-Tethyan slab and asthenosphere upwelling through the slab window would also provide a large amount of heat for the partial melting of thickened mafic lower crust to generate the Napuri adakitic rocks.

Third, dynamic modeling of slab detachment predicts that delay times between the first continental collision and the occurrence of slab break-off range from 10 to 20 m.y. (van Hunen and Allen, 2011). Thus, if break-off of the Neo-Tethyan slab occurred at ca. 51–46 Ma in southern Lhasa, the time at which the Indian continent arrived at the trench (i.e., closure of the Neo-Tethys Ocean) can be estimated at 65–55 Ma. This is consistent with a number of observations. Detailed investigation of upper Cretaceous strata in the Tethys Himalaya also indicated that the initial contact between India and Asia occurred during the Maastrichtian (~70–65 Ma) (Cai et al., 2011). The magnetic anomalies on the Central Indian Ridge and Southeast Indian Ridge (Slater and Fisher, 1974) and palaeomagnetic data (e.g., Lee and Lawver, 1995; White and Lister, 2012) both indicate an India-Eurasia collision in the Paleocene epoch (65–55 Ma). In addition, slab detachment commonly

causes a decrease in convergence rates (e.g., Chung et al., 2005; Lee and Lawver, 1995). The deceleration of the Indian continent relative to Eurasia occurred approximately 50 Ma (e.g., Molnar and Stock, 2009; White and Lister, 2012), broadly coeval with a break-off of the Neo-Tethyan slab at ca. 51–46 Ma.

Fourth, the slab break-off would have led to the cessation of Gangdese arc magmatism and a substantial amount of topographic uplift, similar to that of modern Central America (Rogers et al., 2002). The magmatic quiescence at ca. 45–30 Ma following the Gangdese magmatic peak at ca. 50 Ma probably marked the termination of the Neo-Tethyan oceanic slab subduction (e.g., Chung et al., 2005; Wen et al., 2008a). In addition, an Early Eocene Neo-Tethyan slab breakoff, involving concomitant topographic uplift in southern Tibet (Chung et al., 2005; Kohn and Parkinson, 2002), is consistent with voluminous Early Eocene sediments eroded from the uplifted orogeny in the Bengal basin (Alam et al., 2003).

In summary, the Napuri intrusive rocks were likely produced by partial melting of the mafic lower crust, which was triggered by the upwelling of asthenosphere through the slab window during the break-off of the Neo-Tethyan slab (Fig. 10). In addition, the slab detachment marked the end of the Neo-Tethyan oceanic subduction (e.g., Xu et al., 2008).

5.2.2. Implications for crustal thickening

The adakites defined by Defant and Drummond (1990) are characterized by andesitic-felsic igneous rocks with high Sr and LREEs and low Y and HREEs and high Sr/Y and La/Yb ratios (Castillo, 2012; Martin et al., 2005). These distinctive geochemical features are considered to result from hydrous partial melting of subducted oceanic crust with residual garnet but no plagioclase in the source (Defant and Drummond, 1990).

Recent studies have shown that adakitic rocks can alternatively be generated by partial melting of mafic lower crust (Atherton and Petford, 1993; Chung et al., 2003, 2009; Wang et al., 2007) but the depletion in Y and Yb requires deep crustal melting with garnet as a stable residual phase in their sources (e.g., Atherton and Petford, 1993; Chung et al., 2003, 2009; Wang et al., 2007). Thus, such lower crust-derived adakitic rocks have the potential of tracing the presence of anomalously thick continental crust under the Tibetan plateau (e.g., Chung et al., 2003, 2005, 2009; Guan et al., 2012; Guo et al., 2007; Hou et al., 2004, 2012; Ji et al., 2012 and references therein), and even Cretaceous plateau formation in eastern China (e.g., Zhang et al., 2001). However, some researchers have debated whether an overthickened crust and eclogite residue are necessary for producing adakitic magmas in such a tectonic setting (Ma et al., 2012; Moyen, 2009; Qian and Hermann, 2010). Although numerous melting experiments have demonstrated that partial melting of mafic rocks at 10–38 kbar will generate adakitic melts (e.g., Rapp and Watson, 1995; Rapp et al., 1999, 2003; Xiong, 2006; Xiong et al., 2005, 2009), batch melting modeling indicates that high Sr/Y sources (e.g., the lower crust) could also yield melts with similar high Sr/Y ratios at pressures as low as 5–10 kbar (Ma et al., 2012; Moyen, 2009). Therefore, the significance of the Cenozoic adakitic rocks for crustal thickening in southern Tibet must be carefully evaluated.

Moyen (2009) suggested that high Sr/Y sources could theoretically produce high Sr/Y melts at low pressures (5–10 kbar). Although the presence of residual plagioclase was discussed, effects such as fractional crystallization of plagioclase were not considered in the Moyen (2009) paper. Since plagioclase has high (>2) Kds for Sr (e.g., Blundy et al., 1998; McKenzie and O'Nions, 1991), its fractional crystallization would effectively lower the Sr contents and thus the Sr/Y ratios of the melts. Therefore, partial melting of a high Sr/Y source will often not result in volcanic or plutonic rocks with high Sr/Y ratios. In addition, a high Sr/Y source must also have high La/Yb ratios to generate adakite-like melts with high La/Yb ratios. Moyen's (2009) model has not yet been corroborated by any experimental work. Qian and Hermann (2013) suggested that partial melting of lower crust at 10–15 kbar could

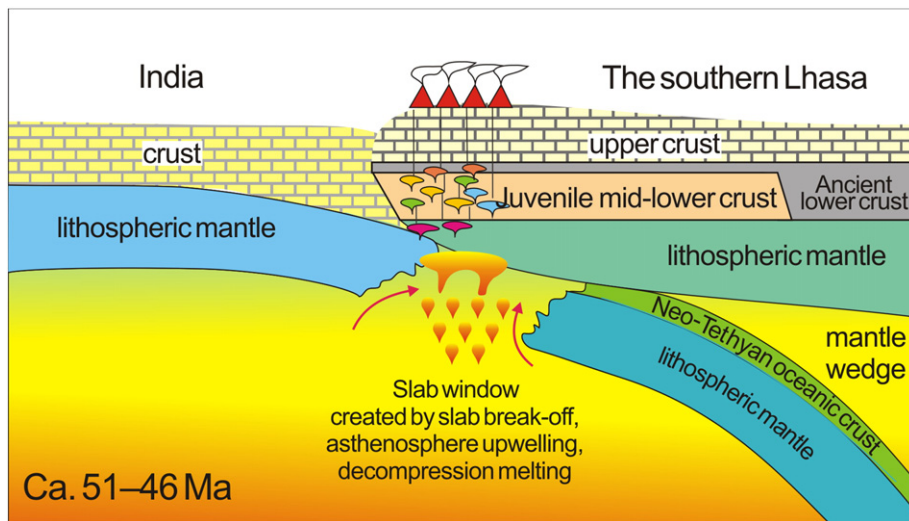


Fig. 10. A suggested model for the formation of the Early Eocene igneous rocks in the southern Lhasa area.

generate adakitic melts but that pressure range corresponds to depths of 30–50 km, thicker than normal continental crust (ca. 30 km, Christensen and Mooney, 1995).

A full accounting of the abundance and inter-element characteristics of trace elements in metabasalt partial melts depends on trace element partitioning between several residual minerals and the melts. As a result, the trace element characteristics of adakitic rocks provide the best constraint on their source mineralogy (Xiong, 2006; Xiong et al., 2005, 2009). HREE are depleted in adakitic magmas derived from subducted slabs because of the presence of residual garnet, which is rich in HREEs, whereas high Sr contents and positive Eu and Sr anomalies indicate no or only minor plagioclase in the residual source (Moyen, 2009; Rapp and Watson, 1995). Garnet is thus a necessary residual mineral for the low HREE and Y contents of adakitic magmas (Defant and Drummond, 1990; Martin, 1999).

Experimental results also have demonstrated that only the presence of residual rutile explains the negative Nb-Ta anomalies in adakitic rocks. Therefore, in addition to garnet, rutile is another key residual mineral (Nair and Chacko, 2008; Xiong, 2006; Xiong et al., 2005). Experimental work indicates that garnet is stable at pressures higher than ~1.0 GPa (Green, 1982), and rutile is stable at pressures higher than ~1.5 GPa (Xiong et al., 2005). Thus, the depth requirement for the presence of both residual garnet and residual rutile is over 50 km (Xiong et al., 2005) (Fig. 11).

Generally, the lower crust has higher Sr/Y ratios and more depleted Nb and Ta contents than mid-ocean ridge basalts (MORB) (Moyen, 2009; Qian and Hermann, 2013; Rudnick and Gao, 2003), which make it difficult to constrain the formation conditions of adakitic magmas (Xiong et al., 2011). In addition, the stability of plagioclase is very sensitive to H_2O content and the breakdown of plagioclase with increasing pressure is a progressive process. Its stability pressure is lower than 1.0 GPa (corresponding to a depth of ~33 km) in the presence of a hydrous fluid, but is up to 1.5–1.8 GPa (corresponding to depths of ~50–60 km) in the case of dehydration melting (e.g., Green, 1982; Rapp and Watson, 1995; Rapp et al., 1999, 2003; Xiong et al., 2011). Therefore, whether residual rutile, garnet and plagioclase occur in the source is the critical factor for constraining the pressure and depth of adakitic melt generation.

The Cenozoic adakitic rocks in southern Lhasa have intermediate to silicic compositions ($SiO_2 = 56\text{--}75\text{ wt.\%}$) (e.g., Chung et al., 2003; Hou et al., 2004; Gao et al., 2007; Guo et al., 2007 and this study). Experiments from 0.3 to 3.2 GPa and 700 to 1150 °C show that the partial

melts of intermediate–felsic rocks are characterized by consistently high SiO_2 contents (>70 wt.%, Xiong et al., 2011). Thus, to account for the full compositional range of the Cenozoic adakitic rocks in southern Lhasa it is necessary that the partial melts were derived from the mafic lower crust. In addition, both Group I Napuri adakitic rocks and some Cenozoic adakitic rocks in southern Lhasa are characterized by positive Eu and Sr anomalies (Fig. 5) (Chung et al., 2003, 2009; Guo et al., 2007; Hou et al., 2004, 2012), indicating that plagioclase was not a residual phase in the source regions of these adakitic rocks.

Xiong et al. (2011) used the SiO_2 versus TiO_2 plot to determine whether these adakitic magmas were saturated with TiO_2 based on experimental data (Rapp and Watson, 1995; Xiong et al., 2005, 2011). Almost all Napuri adakitic rocks plot within the experimental TiO_2 saturation field (Fig. 12), which suggests that the adakitic magmas were saturated in TiO_2 . Nb and Ta fractionation is governed by Ti-enriched minerals (Prowatke and Klemme, 2005). REEs are incompatible in rutile, ilmenite and Ti-magnetite (Prowatke and Klemme, 2005; Xiong et al., 2005). However, these elements are compatible in titanite (Prowatke and Klemme, 2005). Therefore, among Ti-enriched phases, only rutile has the ability to cause a significant decrease in Nb/La in the melt. Garnet is a mineral rich in HREE or Yb, but depleted in light

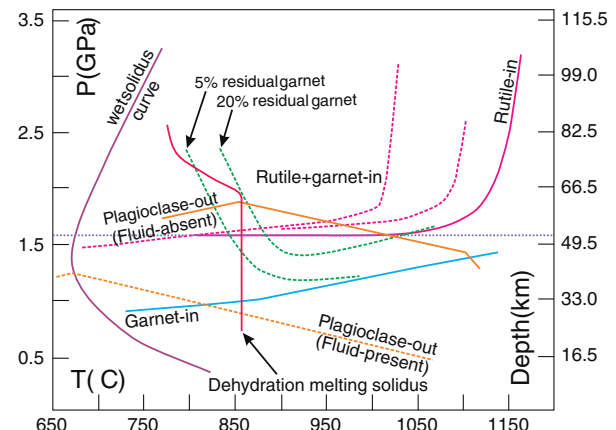


Fig. 11. Phase diagram for continental lower crust with hydrous metabasalt systems. Data sources: Xiong et al. (2005, 2011), Rapp and Watson (1995) and Nair and Chacko (2008).

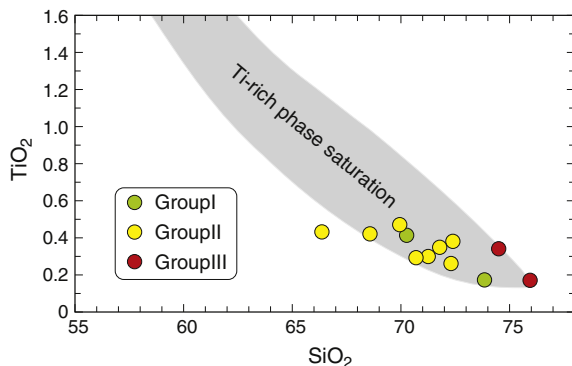


Fig. 12. SiO_2 vs. TiO_2 plot for the Napuri adakitic rocks in southern Lhasa. Shaded area shows the TiO_2 saturation field for partial melting of mafic rocks. After Xiong et al., 2011).

REE or La. Its ability to fractionate La/Yb greatly exceeds that of clinopyroxene and amphibole, and thus an increase in the amount of residual garnet would lead to an increase in La/Yb in the melt. The Napuri adakitic rocks show higher La/Yb (17.3–140, mean = 38.3) and lower Nb/La (0.06–0.38, mean = 0.26) ratios than those ($\text{La}/\text{Yb} = 0.85$ –8.36, mean = 4.19; $\text{Nb}/\text{La} = 0.20$ –0.89, mean = 0.37) of the Cretaceous mafic intrusive rocks, which were suggested to represent the mafic lower crust beneath southern Lhasa (Ma et al., 2013b,c). Collectively, these observations suggest that the Early Eocene Napuri adakitic rocks were derived from source regions with rutile and garnet as the residual minerals, and thus the Early Eocene crustal thickness in southern Lhasa was greater than 50 km (Fig. 11).

Although Early Eocene (Ji et al., 2012) and this study) and Late Cretaceous (Wen et al., 2008b) thickened crust-derived adakitic rocks have previously been recognized in southern Lhasa, different mechanisms were likely involved for the Mesozoic and Cenozoic crustal thickening events. The Mesozoic thickened continental lower crust was mainly formed by the underplating of basaltic magmas related to Neo-Tethyan subduction (e.g., Chung et al., 2009; Dong et al., 2008; Ma et al., 2013b,c; Mo et al., 2007; Wen et al., 2008b). Compared with these Mesozoic crust-derived adakitic rocks (Wen et al., 2008b), the Cenozoic crust-derived adakitic rocks show more enriched Nd–Hf isotopic compositions (Fig. 13a, b) similar to the central Lhasa and the Himalayan basement (e.g., Zhu et al., 2011). The Napuri granitoids, however, are located in the southern Lhasa (Fig. 1), where the Jurassic–Cretaceous (ca. 180–70 Ma) igneous rocks and coeval (ca. 50) gabbros and basalts are characterized by depleted Sr–Nd–Hf isotopic compositions (e.g., Chu et al., 2006; Dong et al., 2008; Ji et al., 2009; Mo et al., 2007, 2008; Wen et al., 2008a, 2008b), indicating that southern Lhasa has a juvenile middle-lower crust that was not a suitable source for the Napuri adakitic rocks. Conversely, there is abundant geochemical data that indicates that the Indian continental lithosphere has subducted beneath the Qiangtang block (e.g., Nábělek et al., 2009; Owens and Zandt, 1997; Schulte-Pelkum et al., 2005) and the Indian crust can be traced to 31°N (Nábělek et al., 2009). Thus, we propose that the enriched isotopic component of Cenozoic crust-derived adakitic rocks results from a significant involvement of the Indian continental crust. Moreover, the most recent study on the Paleocene (~62 Ma) lower crust-derived adakitic rocks in the southern Lhasa block suggests that an enriched Indian crustal component had entered the lower crust beneath the southernmost Lhasa block and that the initial collision between the Indian and Asian blocks had already taken place at that time (Jiang et al., 2014). Thus, the Cenozoic crustal thickening processes beneath southern Lhasa probably involved at least three mechanisms: i) the indentation of India that caused distributed lithospheric thickening with the formation of an orogenic root beneath southern Tibet (Chung et al., 2009); ii) underplating of contemporary and earlier

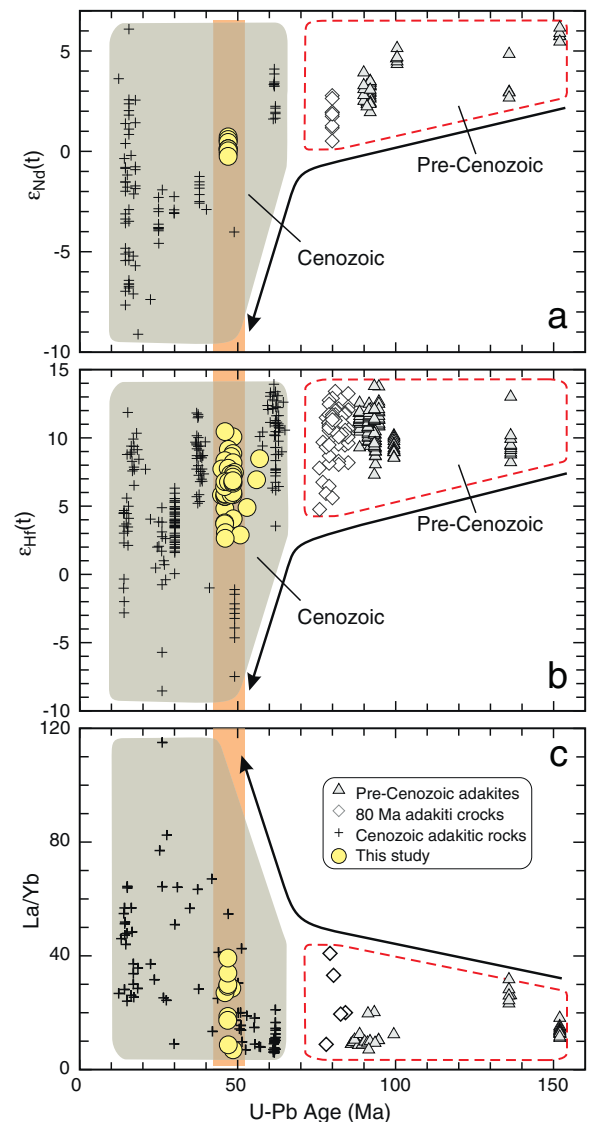


Fig. 13. Plot of (a) $\varepsilon_{\text{Nd}}(t)$, (b) $\varepsilon_{\text{Hf}}(t)$ versus U–Pb ages for the Cretaceous and Cenozoic adakitic rocks in southern Lhasa. Data for the 62 Ma and 152 Ma adakitic rocks are from Jiang et al. (2014) and Wei et al. (2007), respectively. Other data sources are the same as for Fig. 4.

basaltic magmas that generated the juvenile mafic lower crust (e.g., Guan et al., 2012; Lee et al., 2009, 2012; Ma et al., 2013b,c; Mo et al., 2007); iii) melt input from the subducted Indian continental materials as indicated by the significantly decreased Nd–Hf isotopic composition of the magmatic rocks (Chu et al., 2011; Ji et al., 2012).

Along the Andean convergent margin, good correlations have been documented between the REE contents of arc lavas and crustal thickness (e.g., Haschke et al., 2002). Thus, the maximum light/heavy REE ratios have been used to infer the maximum thickness of the Tibetan crust and constrain its evolution (e.g., Chung et al., 2009). Changes in these ratios may be caused by complex petrogenetic processes, including magma mixing, crystal fractionation and upper crustal contamination, in addition to partial melting with residual lower crust garnet that provides a first order control on the REE patterns by retaining heavy REE and Y (Martin, 1999). Accordingly, the sudden changes in $(\text{La}/\text{Yb})_N$ ratios and $\varepsilon_{\text{Nd}}(t)$ values of adakitic rocks in southern Lhasa at ca. 51–46 Ma indicate that the Cenozoic crustal thickening occurred no later than the Early Eocene (ca. 51–46 Ma), and was associated with the Indian collision (Fig. 13). The enriched isotopic compositions of the Napuri adakitic

rocks in southern Lhasa also indicate that the Indian crust had already been subducted beneath the Asian continent by the Early Eocene.

6. Conclusions

The Napuri intrusive rocks were emplaced in the Early Eocene (49–46 Ma), simultaneous with the Early Eocene (ca. 50 Ma) magmatic “flare-up” in southern Lhasa. The Napuri adakitic rocks (Groups I and II) were generated by partial melting of amphibolite eclogites or garnet amphibolites with garnet + rutile ± plagioclase as residual minerals in the source at > 1.5 GPa, corresponding to depths of > 50 km, and the Napuri Group III rocks were probably generated by fractional crystallization of plagioclase from the adakitic magmas. Asthenosphere upwelling triggered by breakoff of the subducted Neo-Tethyan slab is proposed to have provided the required heat for lower crustal melting. Together with the sudden changes in elemental and isotopic compositions of the Gangdese adakites, the results of this study demonstrate that the Cenozoic crustal thickening associated with India's collision with Eurasia began by the Early Eocene (ca. 51–46 Ma).

Acknowledgments

We would like to thank the Editor-in-Chief, Professor Nelson Eby, Professors Sun-Lin Chung and Xiao-Lin Xiong and another anonymous reviewer for their constructive and helpful suggestions. We appreciate the assistance of Yue-Heng Yang, Xi-Rong Liang, Jin-Long Ma, Guang-Qian Hu, Xiang-Lin Tu, Lie-Wen Xie and Ying Liu for the zircon age and geochemical analyses. Financial support for this research was provided by the Strategic Priority Research Program (B) of the Chinese Academy of Sciences (grant no. XDB03010600), the National Natural Science Foundation of China (Nos. 41025006, 41121002 and 41073033) and the Guangzhou Institute of Geochemistry, Chinese Academy of Sciences (GIGCAS 135 project Y234021001). This is contribution No. IS-1838 from GIGCAS, TIGeR publication #511, and contribution 400 from the ARC Centre of Excellence for Core and Crust Fluid Systems (<http://www.ccfs.mq.edu.au>).

References

- Alam, M., Alam, M.M., Curraj, J.R., Chowdhury, M., Gani, M.R., 2003. An overview of the sedimentary geology of the Bengal Basin in relation to the regional tectonic framework and basin-fill history. *Sedimentary Geology* 155, 179–208.
- Arculus, R.J., 2003. Use and abuse of the terms calcalkaline and calcalkalic. *Journal of Petrology* 44 (5), 929–935.
- Atherton, M.P., Petford, N., 1993. Generation of sodium-rich magmas from newly underplated basaltic crust. *Nature* 362, 144–146.
- Bédard, J.H., 2006. Trace element partitioning in plagioclase feldspar. *Geochimica et Cosmochimica Acta* 70, 3717–3742.
- Bindeman, I.N., Davis, A.M., 2000. Trace element partitioning between plagioclase and melt: investigation of dopant influence on partition behavior. *Geochimica et Cosmochimica Acta* 64, 2863–2878.
- Black, L.P., Kamo, S.L., Allen, C.M., Aleinikoff, J.N., Davis, D.W., Korsch, R.J., Foudoulis, C., 2003. TEMORA 1: a new zircon standard for Phanerozoic U-Pb geochronology. *Chemical Geology* 200, 155–170.
- Blundy, J.D., Robinson, J.A.C., Wood, B.J., 1998. Heavy REE are compatible in clinopyroxene on the spinel lherzolite solidus. *Earth and Planetary Science Letters* 160 (3), 493–504.
- Brenan, J., Shaw, H., Ryerson, F., Phinney, D., 1995. Experimental determination of trace-element partitioning between pargasite and a synthetic hydrous andesitic melt. *Earth and Planetary Science Letters* 135, 1–11.
- Cai, F., Ding, L., Yue, Y., 2011. Provenance analysis of upper Cretaceous strata in the Tethys Himalaya, southern Tibet: implications for timing of India–Asia collision. *Earth and Planetary Science Letters* 305 (1), 195–206.
- Castillo, P.R., 2012. Adakite petrogenesis. *Lithos* 134, 304–316.
- Castillo, P.R., Janney, P.E., Solidum, R.U., 1999. Petrology and geochemistry of Camiguin Island, southern Philippines: insights to the source of adakites and other lavas in a complex arc setting. *Contributions to Mineralogy and Petrology* 134, 33–51.
- Chauvel, C., Blachert-Toft, J., 2001. A hafnium isotope and trace element perspective on melting of the depleted mantle. *Earth and Planetary Science Letters* 190, 137–151.
- Chauvel, C., Lewin, E., Carpenterier, M., Arndt, N.T., Marini, J.C., 2008. Role of recycled oceanic basalt and sediment in generating the Hf-Nd mantle array. *Nature Geoscience* 1, 64–67.
- Christensen, N.I., Mooney, W.D., 1995. Seismic velocity structure and composition of the continental crust: a global view. *Journal of Geophysical Research, Solid Earth* 100 (B6), 9761–9788 (1978–2012).
- Chu, M.F., Chung, S.L., Song, B., Liu, D., O'Reilly, S.Y., Pearson, N.J., Ji, J., Wen, D.J., 2006. Zircon U-Pb and Hf isotope constraints on the Mesozoic tectonics and crustal evolution of southern Tibet. *Geology* 34, 745–748.
- Chu, M.-F., Chung, S.-L., O'Reilly, S.Y., Pearson, N.J., Wu, F.-Y., Li, X.-H., Liu, D., Ji, J., Chu, C.-H., Lee, H.-Y., 2011. India's hidden inputs to Tibetan orogeny revealed by Hf isotopes of Transhimalayan zircons and host rocks. *Earth and Planetary Science Letters* 307, 479–486.
- Chung, S.L., Lo, C.H., Lee, T.Y., Zhang, Y., Xie, Y., Li, X., Wang, K.L., Wang, P.L., 1998. Diachronous uplift of the Tibetan plateau starting 40 Myr ago. *Nature* 394, 769–773.
- Chung, S.L., Liu, D., Ji, J., Chu, M.F., Lee, H.Y., Wen, D.J., Lo, C.H., Lee, T.Y., Qian, Q., Zhang, Q., 2003. Adakites from continental collision zones: melting of thickened lower crust beneath southern Tibet. *Geology* 31, 1021–1024.
- Chung, S.L., Chu, M.F., Zhang, Y., Xie, Y., Lo, C.H., Lee, T.Y., Lan, C.Y., Li, X., Zhang, Q., Wang, Y., 2005. Tibetan tectonic evolution inferred from spatial and temporal variations in post-collisional magmatism. *Earth-Science Reviews* 68, 173–196.
- Chung, S.L., Chu, M.F., Ji, J., O'Reilly, S.Y., Pearson, N., Liu, D., Lee, T.Y., Lo, C.H., 2009. The nature and timing of crustal thickening in Southern Tibet: geochemical and zircon Hf isotopic constraints from postcollisional adakites. *Tectonophysics* 477, 36–48.
- Coulon, C., Maluski, H., Bollinger, C., Wang, S., 1986. Mesozoic and Cenozoic volcanic rocks from central and southern Tibet: ^{39}Ar – ^{40}Ar dating, petrological characteristics and geodynamical significance. *Earth and Planetary Science Letters* 79, 281–302.
- Davies, J.H., von Blanckenburg, F., 1995. Slab breakoff: a model of lithosphere detachment and its test in the magmatism and deformation of collisional orogens. *Earth and Planetary Science Letters* 129, 85–102.
- Defant, M.J., Drummond, M.S., 1990. Derivation of some modern arc magmas by melting of young subducted lithosphere. *Nature* 347, 662–665.
- DePaolo, D.J., 1988. Neodymium Isotope Geochemistry: An Introduction. Springer, New York (181 pp.).
- Dong, G.C., Mo, X.X., Zhao, Z.D., Zhu, D.C., Song, Y.T., Wang, L., 2008. Gabbros from Southern Gangdese: implication for mass exchange between mantle and crust. *Acta Petrologica Sinica* 24 (2), 203–210 (in Chinese with English Abstract).
- Gao, Y., Hou, Z., Kamber, B.S., Wei, R., Meng, X., Zhao, R., 2007. Adakite-like porphyries from the southern Tibetan continental collision zones: evidence for slab melt metasomatism. *Contributions to Mineralogy and Petrology* 153, 105–120.
- Gao, Y., Yang, Z., Santosh, M., Hou, Z., Wei, R., Tian, S., 2010. Adakitic rocks from slab melt-modified mantle sources in the continental collision zone of southern Tibet. *Lithos* 119, 651–663.
- Green, T.H., 1982. Anatexis of mafic crust and high pressure crystallization of andesite. In: Thorpe, R.S. (Ed.), *Andesites: Orogenic Andesites and Related Rocks*. John Wiley and Sons, New York, pp. 465–487.
- Guan, Q., Zhu, D.C., Zhao, Z.D., Zhang, L.L., Liu, M., Li, X.W., Yu, F., Mo, X.X., 2010. Late Cretaceous adakites in the eastern segment of the Gangdese Belt, southern Tibet: products of Neo-Tethyan ridge subduction? *Acta Petrologica Sinica* 26, 2165–2179.
- Guan, Q., Zhu, D.C., Zhao, Z.D., Dong, G.C., Zhang, L.L., Li, X.W., Liu, M., Mo, X.X., Liu, Y.S., Yuan, H.L., 2012. Crustal thickening prior to 38 Ma in southern Tibet: evidence from lower crust-derived adakitic magmatism in the Gangdese Batholith. *Gondwana Research* 21, 88–99.
- Guo, Z., Wilson, M., 2012. The Himalayan leucogranites: constraints on the nature of their crustal source region and geodynamic setting. *Gondwana Research* 22, 360–376.
- Guo, Z., Wilson, M., Liu, J., Mao, Q., 2006. Post-collisional, potassic and ultrapotassic magmatism of the northern Tibetan Plateau: constraints on characteristics of the mantle source, geodynamic setting and uplift mechanisms. *Journal of Petrology* 47, 1177.
- Guo, Z., Wilson, M., Liu, J., 2007. Post-collisional adakites in south Tibet: products of partial melting of subduction-modified lower crust. *Lithos* 96, 205–224.
- Harris, N., Ronghua, X., Lewis, C., Hawkesworth, C., Yuquan, Z., 1988. Isotope geochemistry of the 1985 Tibet geotraverse, Lhasa to Golmud. *Philosophical Transactions of the Royal Society of London. Series A: Mathematical and Physical Sciences* 327, 263–285.
- Haschke, M., Siebel, W., Günther, A., Scheuber, E., 2002. Repeated crustal thickening and recycling during the Andean orogeny in north Chile (21°–26°S). *Journal of Geophysical Research* 107. <http://dx.doi.org/10.1029/2001JB000328>.
- He, Y., Li, S., Hoefs, J., Huang, F., Liu, S.A., Hou, Z., 2011. Post-collisional granitoids from the Dabie orogen: new evidence for partial melting of a thickened continental crust. *Geochimica et Cosmochimica Acta* 75 (13), 3815–3838.
- Hoskin, P., Black, L., 2000. Metamorphic zircon formation by solid state recrystallization of protolith igneous zircon. *Journal of Metamorphic Geology* 18, 423–439.
- Hou, Z.Q., Gao, Y.F., Qu, X.M., Rui, Z.Y., Mo, X.X., 2004. Origin of adakitic intrusives generated during mid-Miocene east–west extension in southern Tibet. *Earth and Planetary Science Letters* 220, 139–155.
- Hou, Z.Q., Zheng, Y.C., Zeng, L.S., Gao, L.E., Huang, K.X., Li, W., Li, Q.Y., Fu, Q., Liang, W., Sun, Q.Z., 2012. Eocene–Oligocene granitoids in southern Tibet: constraints on crustal anatexis and tectonic evolution of the Himalayan orogeny. *Earth and Planetary Science Letters* 349–350, 38–52.
- Huang, F., He, Y.S., 2010. Partial melting of the dry mafic continental crust: implications for petrogenesis of C-type adakites. *Chinese Science Bulletin* 55, 2428–2439.
- Huang, X.L., Xu, Y.G., Lo, C.H., Wang, R.C., Lin, C.Y., 2007. Exsolution lamellae in a clinopyroxene megacryst aggregate from Cenozoic basalt, Leizhou Peninsula, South China: petrography and chemical evolution. *Contributions to Mineralogy and Petrology* 154, 691–705.
- Ingle, S., Weis, D., Doucet, S., Mattielli, N., 2003. Hf isotope constraints on mantle sources and shallow-level contaminants during Kerguelan hot spot activity since 120 Ma. *Geochemistry, Geophysics, Geosystems* 4, 1068. <http://dx.doi.org/10.1029/2002GC000482>.
- Ji, W.Q., Wu, F.Y., Chung, S.L., Li, J.X., Liu, C.Z., 2009. Zircon U-Pb geochronology and Hf isotopic constraints on petrogenesis of the Gangdese batholith, southern Tibet. *Chemical Geology* 262, 229–245.

- Ji, W.Q., Wu, F.Y., Liu, C.Z., Chung, S.L., 2012. Early Eocene crustal thickening in southern Tibet: new age and geochemical constraints from the Gangdese batholith. *Journal of Asian Earth Sciences* 53, 82–95.
- Jiang, Z.Q., Wang, Q., Wyman, D.A., Tang, G.J., Jia, X.H., Yang, Y.H., Yu, H.X., 2011. Origin of 30 Ma Chongmuda adakitic intrusive rocks in the southern Gangdese region, southern Tibet: partial melting of the northward subducted Indian continent crust? *Geochimica* 40, 126–146 (in Chinese with English abstract).
- Jiang, Z.Q., Wang, Q., Li, Z.X., Wyman, D.A., Tang, G.J., Jia, X.H., Yang, Y.H., 2012. Late Cretaceous (ca. 90 Ma) adakitic intrusive rocks in the Kelu area, Gangdese belt (southern Tibet): slab melting and implications for Cu–Au mineralization. *Journal of Asian Earth Sciences* 53, 67–81.
- Jiang, Z.Q., Wang, Q., Wyman, D.A., Li, Z.X., Yang, J.H., Shi, X.B., Tang, G.J., Jia, X.H., Ma, L., Gou, G.N., Guo, H.F., 2014. Transition from oceanic to continental lithosphere subduction in southern Tibet: Evidence from the Late Cretaceous–Early Oligocene (~91–30 Ma) intrusive rocks in the Chanang–Zedong area, southern Gangdese. *Lithos* 196–197, 213–231.
- Kamei, A., Miyake, Y., Owada, M., Kimura, J.I., 2009. A pseudo adakite derived from partial melting of tonalitic to granodioritic crust, Kyushu, southwest Japan arc. *Lithos* 112, 615–625.
- King, J., Harris, N., Argles, T., Parrish, R., Charlier, B., Sherlock, S., Zhang, H.F., 2007. First field evidence of southward ductile flow of Asian crust beneath southern Tibet. *Geology* 35, 727.
- Klein, M., Stosch, H.G., Seck, H.A., Shimizu, N., 2000. Experimental partitioning of high field strength and rare earth elements between clinopyroxene and garnet in andesitic to tonalitic systems. *Geochimica et Cosmochimica Acta* 64 (1), 99–115.
- Kohn, M.J., Parkinson, C.D., 2002. Petrologic case for Eocene slab breakoff during the Indo-Asian collision. *Geology* 30 (7), 591–594.
- Lee, T.Y., Lawver, L.A., 1995. Cenozoic plate reconstruction of Southeast Asia. *Tectonophysics* 251 (1), 85–138.
- Lee, H.Y., Chung, S.L., Lo, C.H., Ji, J., Lee, T.Y., Qian, Q., Zhang, Q., 2009. Eocene Neotethyan slab breakoff in southern Tibet inferred from the Linzizong volcanic record. *Tectonophysics* 477, 20–35.
- Lee, H.Y., Chung, S.L., Ji, J.Q., Qian, Q., Galleta, S., Lo, C.H., Lee, T.Y., Zhang, Q., 2012. Geochemical and Sr–Nd isotopic constraints on the genesis of the Cenozoic Linzizong volcanic successions, southern Tibet. *Journal of Asian Earth Sciences* 53, 96–114.
- Li, X.H., Zhou, H., Chung, S.L., Lo, C.H., Wei, G., Liu, Y., Lee, C.Y., 2002. Geochemical and Sr–Nd isotopic characteristics of late Paleogene ultrapotassic magmatism in southeastern Tibet. *International Geology Review* 44, 559–574.
- Li, X.H., Liu, D., Sun, M., Li, W.X., Liang, X.R., Liu, Y., 2004. Precise Sm–Nd and U–Pb isotopic dating of the supergiant Shizhuayan polymetallic deposit and its host granite, SE China. *Geological Magazine* 141, 225.
- Li, X.H., Qi, C.S., Liu, Y., Liang, X.R., Tu, X.L., Xie, L.W., Yang, Y.H., 2005. Petrogenesis of the Neoproterozoic bimodal volcanic rocks along the western margin of the Yangtze Block: new constraints from Hf isotopes and Fe/Mn ratios. *Chinese Science Bulletin* 50, 2481–2486.
- Ludwig, K., 2001. SQUID 1.02, A User's Manual, 2. Berkeley Geochronological Center 2455 (Special Publication).
- Ma, Q., Zheng, J.P., Griffin, W.L., Tang, H.Y., Su, Y.P., Ping, X.Q., 2012. Triassic “adakitic” rocks in an extensional setting (North China): melts from the cratonic lower crust. *Lithos* 149, 159–173.
- Ma, L., Wang, Q., Wyman, D.A., Li, Z.-X., Jiang, Z.-Q., Yang, J.-H., Gou, G.-N., Guo, H.-F., 2013a. Late Cretaceous (100–89 Ma) magnesian charnockites with adakitic affinities in the Milin area, eastern Gangdese: partial melting of subducted oceanic crust and implications for crustal growth in southern Tibet. *Lithos* 175–176, 315–332.
- Ma, L., Wang, Q., Wyman, D.A., Jiang, Z.Q., Yang, J.H., Li, Q.L., Gou, G.N., Guo, H.F., 2013b. Late Cretaceous crustal growth in the Gangdese area, southern Tibet: petrological and Sr–Nd–Hf–O isotopic evidence from Zhengga diorite–gabbro. *Chemical Geology* 349–350, 54–70.
- Ma, L., Wang, Q., Li, Z.X., Wyman, D.A., Jiang, Z.Q., Yang, J.H., Gou, G.N., Guo, H.F., 2013c. Early Late Cretaceous (ca. 93 Ma) norites and hornblendites in the Milin area, eastern Gangdese: lithosphere–asthenosphere interaction during slab roll-back and an insight into early Late Cretaceous (ca. 100–80 Ma) magmatic “flare-up” in southern Lhasa (Tibet). *Lithos* 172–173, 17–30.
- Macpherson, C.G., Dreher, S.T., Thirlwall, M.F., 2006. Adakites without slab melting: high pressure differentiation of island arc magma, Mindanao, the Philippines. *Earth and Planetary Science Letters* 243, 581–593.
- Maniar, P.D., Piccoli, P.M., 1989. Tectonic discrimination of granitoids. *Geological Society of America Bulletin* 101, 635–643.
- Martin, H., 1999. Adakitic magmas: modern analogues of Archaean granitoids. *Lithos* 46, 411–429.
- Martin, H., Smithies, R., Rapp, R., Moyen, J.F., Champion, D., 2005. An overview of adakite, tonalite–trondhjemite–granodiorite (TTG), and sanukitoid: relationships and some implications for crustal evolution. *Lithos* 79, 1–24.
- McKenzie, D., O'niions, R., 1991. Partial melt distributions from inversion of rare earth element concentrations. *Journal of Petrology* 32, 1021–1091.
- Middlemost, E.A.K., 1994. Naming materials in the magma/igneous rock system. *Earth-Science Reviews* 37, 215–224.
- Miyashiro, A., 1974. Volcanic rock series in island arcs and active continental margins. *American Journal of Science* 274, 321–355.
- Mo, X., Niu, Y., Dong, G., Zhao, Z., Hou, Z., Zhou, S., Ke, S., 2008. Contribution of syncollisional felsic magmatism to continental crust growth: a case study of the Paleogene Linzizong volcanic succession in southern Tibet. *Chemical Geology* 250, 49–67.
- Mo, X., Hou, Z., Niu, Y., Dong, G., Qu, X., Zhao, Z., Yang, Z., 2007. Mantle contributions to crustal thickening during continental collision: evidence from Cenozoic igneous rocks in southern Tibet. *Lithos* 96 (1), 225–242.
- Molnar, P., Stock, J.M., 2009. Slowing of India's convergence with Eurasia since 20 Ma and its implications for Tibetan mantle dynamics. *Tectonics* 28, TC3001. <http://dx.doi.org/10.1029/2008TC002271>.
- Moyen, J.F., 2009. High Sr/Y and La/Yb ratios: the meaning of the “adakitic signature”. *Lithos* 112, 556–574.
- Nábělek, J., Hetényi, G., Vergne, J., Sapkota, S., Kafle, B., Jiang, M., Su, H., Chen, J., Huang, B.-S., Team, t.-H.C., 2009. Underplating in the Himalaya–Tibet Collision Zone Revealed by the Hi-CLIMB Experiment. *Science* 325, 1371–1374.
- Nair, R., Chacko, T., 2008. Role of oceanic plateaus in the initiation of subduction and origin of continental crust. *Geology* 36, 583–586.
- Owens, T.J., Zandt, G., 1997. Implications of crustal property variations for models of Tibetan plateau evolution. *Nature* 387, 37–43.
- Pan, F.B., Zhang, H.F., Harris, N., Xu, W.C., Guo, L., 2012. Oligocene magmatism in the eastern margin of the east Himalayan syntaxis and its implication for the India–Asia post-collisional process. *Lithos* 154, 181–192.
- Peccerillo, A., Taylor, S., 1976. Geochemistry of Eocene calc-alkaline volcanic rocks from the Kastamonu area, northern Turkey. *Contributions to Mineralogy and Petrology* 58, 63–81.
- Petford, N., Atherton, M., 1996. Na-rich partial melts from newly underplated basaltic crust: the Cordillera Blanca Batholith, Peru. *Journal of Petrology* 37, 1491–1521.
- Pidgeon, R., Furfaro, D., Kennedy, A., Nemchin, A., Van Bronswijk, W., Todt, W., 1994. Calibration of zircon standards for the Curtin SHRIMP II. Eighth International Conference on Geochronology, Cosmochemistry and Isotope Geology: US Geological Survey Circular, p. 251.
- Prowatke, S., Klemme, S., 2005. Effect of melt composition on the partitioning of trace elements between titanite and silicate melt. *Geochimica et Cosmochimica Acta* 69, 695–709.
- Qian, Q., Hermann, J., 2010. Formation of high-Mg diorites through assimilation of peridotite by monzodiorite magma at crustal depths. *Journal of Petrology* 51 (7), 1381–1416.
- Qian, Q., Hermann, J., 2013. Partial melting of lower crust at 10–15 kbar: constraints on adakite and TTG formation. *Contributions to Mineralogy and Petrology* 165, 1195–1224.
- Rapp, R.P., Watson, E.B., 1995. Dehydration melting of metabasalt at 8–32 kbar: implications for continental growth and crust–mantle recycling. *Journal of Petrology* 36, 891–931.
- Rapp, R., Shimizu, N., Norman, M., Applegate, G., 1999. Reaction between slab-derived melts and peridotite in the mantle wedge: experimental constraints at 3.8 GPa. *Chemical Geology* 160, 335–356.
- Rapp, R.P., Shimizu, N., Norman, M.D., 2003. Growth of early continental crust by partial melting of eclogite. *Nature* 425, 605–609.
- Rogers, R.D., Kárasón, H., van der Hilst, R.D., 2002. Epeirogenic uplift above a detached slab in northern Central America. *Geology* 30 (11), 1031–1034.
- Royden, L.H., Burchfiel, B.C., King, R.W., Wang, E., Chen, Z., Shen, F., Liu, Y., 1997. Surface deformation and lower crustal flow in eastern Tibet. *science* 276 (11), 788–790.
- Rudnick, R., Gao, S., 2003. Composition of the continental crust. *Treatise on Geochemistry* 3, 1–64.
- Schulte-Pelkum, V., Monsalve, G., Sheehan, A., Pandey, M., Sapkota, S., Bilham, R., Wu, F., 2005. Imaging the Indian subcontinent beneath the Himalaya. *Nature* 435, 1222–1225.
- Slater, J.G., Fisher, R.L., 1974. Evolution of the east: Central Indian Ocean, with emphasis on the tectonic setting of the Ninetyeast Ridge. *Geological Society of America Bulletin* 85, 683–702.
- Shimoda, G., Tatsumi, Y., Nohda, S., Ishizaka, K., Jahn, B., 1998. Setouchi high-Mg andesites revisited: geochemical evidence for melting of subducting sediments. *Earth and Planetary Science Letters* 160, 479–492.
- Soderlund, U., Patchett, P.J., Vervoort, J.D., Isachsen, C.E., 2004. The 176Lu decay constant determined by Lu–Hf and U–Pb isotope systematics of Precambrian mafic intrusions. *Earth and Planetary Science Letters* 219 (3), 311–324.
- Stacey, J.S., Kramers, J., 1975. Approximation of terrestrial lead isotope evolution by a two-stage model. *Earth and Planetary Science Letters* 26, 207–221.
- Stern, C.R., Kilian, R., 1996. Role of the subducted slab, mantle wedge and continental crust in the generation of adakites from the Andean Austral Volcanic Zone. *Contributions to Mineralogy and Petrology* 123, 263–281.
- Streck, M.J., Leeman, W.P., Chesley, J., 2007. High-Mg andesite from Mount Shasta: a product of magma mixing and contamination, not a primitive mantle melt. *Geology* 35, 351–354.
- Sun, S.S., McDonough, W., 1989. Chemical and isotopic systematics of oceanic basalts: implications for mantle composition and processes. *Geological Society, London, Special Publications* 42, 313–345.
- Tapponnier, P., Zhiqin, X., Roger, F., Meyer, B., Arnaud, N., Wittlinger, G., Jingsui, Y., 2001. Oblique stepwise rise and growth of the Tibet Plateau. *Science* 294, 1671–1677.
- Tatsumi, Y., 2006. High-Mg andesites in the Setouchi Volcanic Belt, Southwestern Japan: analogy to Archean magmatism and continental crust formation? *Annual Review of Earth and Planetary Sciences* 34, 467–499.
- Turner, S., Arnaud, N., Liu, J., Rogers, N., Hawkesworth, C., Harris, N., Kelley, S., Van Calsteren, P., Deng, W., 1996. Post-collision, shoshonitic volcanism on the Tibetan Plateau: implications for convective thinning of the lithosphere and the source of ocean island basalts. *Journal of Petrology* 37, 45–71.
- van Hunen, J., Allen, M.B., 2011. Continental collision and slab break-off: a comparison of 3-D numerical models with observations. *Earth and Planetary Science Letters* 302 (1), 27–37.
- von Blanckenburg, F., Davis, J.H., 1995. Slab breakoff: a model for syncollisional magmatism and tectonics in the Alps. *Tectonics* 14, 120–131.
- Wang, Q., McDermott, F., Xu, J.F., Bellon, H., Zhu, Y.T., 2005. Cenozoic K-rich adakitic volcanic rocks in the Hohxil area, northern Tibet: lower crustal melting in an intracontinental setting. *Geology* 33, 464–468.

- Wang, Q., Xu, J.F., Jian, P., Bao, Z.W., Zhao, Z.H., Li, C.F., Xiong, X.L., Ma, J.L., 2006. Petrogenesis of adakitic porphyries in an extensional tectonic setting, Dexing, South China: implications for the genesis of porphyry copper mineralization. *Journal of Petrology* 47, 119–144.
- Wang, Q., Wyman, D.A., Xu, J., Jian, P., Zhao, Z., Li, C., Xu, W., Ma, J., He, B., 2007. Early Cretaceous adakitic granites in the Northern Dabie Complex, central China: implications for partial melting and delamination of thickened lower crust. *Geochimica et Cosmochimica Acta* 71, 2609–2636.
- Wang, Q., Wyman, D.A., Xu, J., Dong, Y., Vasconcelos, P.M., Pearson, N., Wan, Y., Dong, H., Li, C., Yu, Y., Zhu, T., Feng, X., Zhang, Q., Zi, F., Chu, Z., 2008. Eocene melting of subducting continental crust and early uplifting of central Tibet: evidence from central-western Qiangtang high-K calc-alkaline andesites, dacites and rhyolites. *Earth and Planetary Science Letters* 272, 158–171.
- Wang, Q., Chung, S.L., Li, X.H., Wyman, D.A., Li, Z.X., Sun, W.D., Qiu, H.N., Liu, Y.S., Zhu, Y.T., 2012. Crustal melting and flow beneath Northern Tibet: evidence from Mid-Miocene to Quaternary strongly peraluminous rhyolites in the Southern Kunlun Range. *Journal of Petrology* 53 (12), 2523–2566.
- Watson, E.B., Harrison, T.M., 1983. Zircon saturation revisited: temperature and composition effects in a variety of crustal magma types. *Earth and Planetary Science Letters* 64, 295–304.
- Wei, G.J., Liang, X.R., Li, X.H., Liu, Y., 2002. Precise measurement of Sr isotopic compositions of liquid and solid base using (LP) MCICP-MS. *Geochimica* 31, 295–305 (in Chinese with English abstract).
- Wei, D.L., Xia, B., Zhou, G.Q., Yan, J., Wang, R., Zhong, L.F., 2007. Geochemical and Sr-Nd isotopic characteristics of tonalite rock in Zedang area, Tibet: new evidences for Tethys subduction. *Science in China Series D-Earth Sciences* 37 (4), 442–450.
- Wen, D.R., Liu, D., Chung, S.L., Chu, M.F., Ji, J., Zhang, Q., Song, B., Lee, T.Y., Yeh, M.W., Lo, C.H., 2008a. Zircon SHRIMP U-Pb ages of the Gangdese Batholith and implications for Neotethyan subduction in southern Tibet. *Chemical Geology* 252, 191–201.
- Wen, D.R., Chung, S.L., Song, B., Iizuka, Y., Yang, H.J., Ji, J., Liu, D., Gallet, S., 2008b. Late Cretaceous Gangdese intrusions of adakitic geochemical characteristics, SE Tibet: petrogenesis and tectonic implications. *Lithos* 105, 1–11.
- White, L.T., Lister, G.S., 2012. The collision of India with Asia. *Journal of Geodynamics* 56, 7–17.
- Williams, I., 1998. U-Th-Pb geochronology by ion microprobe. *Reviews in Economic Geology* 7, 1–35.
- Wu, F.Y., Yang, Y.H., Xie, L.W., Yang, J.H., Xu, P., 2006. Hf isotopic compositions of the standard zircons and baddeleyites used in U-Pb geochronology. *Chemical Geology* 234, 105–126.
- Xie, L.W., Zhang, Y.B., Zhang, H.H., Sun, J.F., Wu, F.Y., 2008. In situ simultaneous determination of trace elements, U-Pb and Lu-Hf isotopes in zircon and baddeleyite. *Chinese Science Bulletin* 53, 1565–1573.
- Xiong, X.L., 2006. Trace element evidence for the growth of early continental crust by melting of rutile-bearing hydrous eclogite. *Geology* 34, 945–948.
- Xiong, X.L., Adam, J., Green, T.H., 2005. Rutile stability and rutile/melt HFSE partitioning during partial melting of hydrous basalt: implications for TTG genesis. *Chemical Geology* 218, 339–359.
- Xiong, X.L., Keppler, H., Audébat, A., Gudfinnsson, G., Sun, W.D., Song, M.S., Xiao, W.S., Yuan, L., 2009. Experimental constraints on rutile saturation during partial melting of metabasalt at the amphibolite to eclogite transition, with applications to TTG genesis. *American Mineralogist* 94, 1175–1186.
- Xiong, X.L., Liu, X.C., Zhu, Z.M., Xiao, W.S., Song, M.S., Zhang, S., Wu, W.S., 2011. Adakitic rocks and destruction of the North China Craton: evidence from experimental petrology and geochemistry. *Science China Earth Science* 54, 858–870.
- Xu, J.F., Castillo, P.R., 2004. Geochemical and Nd-Pb isotopic characteristics of the Tethyan asthenosphere: implications for the origin of the Indian Ocean mantle domain. *Tectonophysics* 393, 9–27.
- Xu, Y.G., Lan, J.B., Yang, Q.J., Huang, X.L., Qiu, H.N., 2008. Eocene break-off of the Neo-Tethyan slab as inferred from intraplate-type mafic dykes in the Gaoligong orogenic belt, eastern Tibet. *Chemical Geology* 255, 439–453.
- Xu, W.C., Zhang, H.F., Guo, L., Yuan, H.L., 2010. Miocene high Sr/Y magmatism, south Tibet: product of partial melting of subducted Indian continental crust and its tectonic implication. *Lithos* 114, 293–306.
- Yin, A., Harrison, T.M., 2000. Geologic evolution of the Himalayan–Tibetan orogen. *Annual Review of Earth and Planetary Sciences* 28, 211–280.
- Zeng, L.S., Gao, L.E., Xie, K.J., Liu-Zeng, J., 2011. Mid-Eocene high Sr/Y granites in the Northern Himalayan Gneiss Domes: melting thickened lower continental crust. *Earth and Planetary Science Letters* 303, 251–266.
- Zhang, Q., Qian, Q., Wang, E.Q., Wang, Y., Zhao, T.P., Hao, J., Guo, G.J., 2001. An East China Plateau in mid-late Yanshanian period: implication from adakites. *Chinese Journal of Geology* 36, 248–255 (in Chinese with English abstract).
- Zhang, H., Harris, N., Guo, L., Xu, W., 2010a. The significance of Cenozoic magmatism from the western margin of the eastern syntaxis, southeast Tibet. *Contributions to Mineralogy and Petrology* 160, 83–98.
- Zhang, Z.M., Zhao, G.C., Santosh, M., Wang, J.L., Dong, X., Shen, K., 2010b. Late Cretaceous charnockite with adakitic affinities from the Gangdese batholith, southeastern Tibet: evidence for Neo-Tethyan mid-ocean ridge subduction? *Gondwana Research* 17, 615–631.
- Zhu, D.C., Pan, G.T., Chung, S.L., Liao, Z.L., Wang, L.Q., Li, G.M., 2008. SHRIMP zircon age and geochemical constraints on the origin of Lower Jurassic volcanic rocks from the Yeba Formation, southern Gangdese, South Tibet. *International Geology Review* 50, 442–471.
- Zhu, D.C., Zhao, Z.D., Pan, G.T., Lee, H.Y., Kang, Z.Q., Liao, Z.L., Wang, L.Q., Li, G.M., Dong, G.C., Liu, B., 2009. Early cretaceous subduction-related adakite-like rocks of the Gangdese Belt, southern Tibet: products of slab melting and subsequent melt-peridotite interaction? *Journal of Asian Earth Sciences* 34, 298–309.
- Zhu, D.C., Zhao, Z.D., Niu, Y.L., Mo, X.X., Chung, S.L., Hou, Z.Q., Wang, L.Q., Wu, F.Y., 2011. The Lhasa Terrane: record of a microcontinent and its histories of drift and growth. *Earth and Planetary Science Letters* 301, 241–255.
- Zhu, D.C., Zhao, Z.D., Niu, Y., Dilek, Y., Hou, Z.Q., Mo, X.X., 2013. The origin and pre-Cenozoic evolution of the Tibetan Plateau. *Gondwana Research* 23, 1429–1454.